Tissue acidosis associated with ischemic stroke to guide nimodipine delivery

PhD Thesis

Orsolya M Tóth MD

Szeged, 2021

University of Szeged

Faculty of Medicine, Faculty of Science and Informatics

Department of Medical Physics and Informatics

Tissue acidosis associated with ischemic stroke to guide nimodipine delivery

PhD Thesis

Orsolya M Tóth MD

Supervisors:
Eszter Farkas D. Sc. and Prof. Ferenc Bari D. Sc.

Doctoral School of Theoretical Medicine

Szeged, 2021

Publications related to the PhD thesis:

I. Szabó Í, **M Tóth O**, Török Z, Varga DP, Menyhárt Á, Frank R, Hantosi D, Hunya Á, Bari F, Horváth I, Vigh L, Farkas E. The impact of dihydropyridine derivatives on the cerebral blood flow response to somatosensory stimulation and spreading depolarization. Br J Pharmacol. 2019 May;176(9):1222-1234. *doi: 10.1111/bph.14611*. **IF: 7.73**

II. **M Tóth O**, Menyhárt Á, Varga VÉ, Hantosi D, Ivánkovits-Kiss O, Varga DP, Szabó Í, Janovák L, Dékány I, Farkas E, Bari F. Chitosan nanoparticles release nimodipine in response to tissue acidosis to attenuate spreading depolarization evoked during forebrain ischemia. Neuropharmacology. 2020 Jan 1;162:107850. *doi: 10.1016/j.neuropharm.2019.107850*. **IF: 4.431**

III. **M Tóth O**, Menyhárt Á, Frank R, Hantosi D, Farkas E, Bari F. Tissue Acidosis Associated with Ischemic Stroke to Guide Neuroprotective Drug Delivery. Biology (Basel). 2020 Dec 11;9(12):460. *doi: 10.3390/biology9120460*. **IF: 3.796**

Abbreviations

2VO: 2-vessel occlusion (transient bilateral common carotid artery occlusion)

aCSF: artificial cerebrospinal fluid

AMPA: α-amino-3-hydroxy-5-methyl-4-isoxazolepropionic acid

ANOVA: analysis of variance

ATP: Adenosine-tryphosphate

AUC: area under the curve

B: branches/grid intersections

BBB: blood-brain barrier

CBD: microglial cell bodies within the grid

CBF: cerebral blood flow

CL: contralateral

CT: computer tomography

DAB: diaminobenzidine

DC potential: direct current potential or slow cortical potential

DDS: drug delivery system

DMSO: dimethyl-sulfoxide

DNA: Deoxyribonucleic acid

EFP: evoked field potential

EU: European Union

HEPES: 4-(2-hydroxyethyl)-1-piperazineethanesulfonic acid

HVA and LVA: high and low voltage-activated channels

Iba1: ionized calcium binding adaptor molecule 1

IL: ipsilateral

LDF: Laser Doppler flowmetry

LFP: local field potential

MABP: middle arterial blood pressure

MCAO: middle cerebral artery occlusion

MRI: magnetic resonance imaging

N_2O: nitrous oxide

NCX: Na-Ca exchanger

NeuN: neuronal nuclei

NMDA: N-methyl-D-aspartate

nNOS: NO synthase

NO: nitric oxide

NP: nanoparticle

O_2: molecular oxygen

pCO_2: partial pressure of CO_2

PET: Positron emitted tomography

PFA: paraformaldehyde

PMCA: plasma membrane Ca ATPase

RI: ramification index

ROS: reactive oxygen species

rSD: recurrent SD

SAH: subarachnoid hemorrhage

SD: spreading depolarization

stdev: standard deviation

VGCC: voltage-gated Ca^{2+} channels

VSMC: vascular smooth muscle cell

4

Contents

1. Introduction

Nowadays cerebrovascular diseases are the second most frequent cause of death and the most common cause of long-term disability worldwide [1]. Despite this global health problem, there are only limited therapeutic possibilities, and none of them is effective for every stroke patient. It would be desirable for the medical treatment to target the site of injury selectively, to enrich the site of ongoing injury with the protective agent, and to avoid undesirable side effects at the same time. We propose that ischemia-induced acid accumulation can be utilized to target drug release from nanocarriers. Our aim was to investigate (i) whether tissue acidosis caused by ischemia initiates drug release from specific carriers in the nervous tissue, and (ii) whether nimodipine administered with nanoparticles exerts its expected vasodilator and neuroprotective effect. Ultimately, this approach may offer a new way to treat stroke patients with the hope of more effective therapy, and better stroke outcome than achievable at present.

1.1. Mechanistic insight into cellular pathomechanisms of ischemic stroke

1.1.1. Disrupted ion homeostasis under cerebral ischemia

Because of its high metabolic rate and limited storage capacity for oxygen and glucose, the brain is extremely vulnerable to ischemia [2]. Global cerebral ischemia, a complete cessation of blood supply to the brain is mainly associated with cardiac arrest or cardiac surgery. Conversely, focal cerebral ischemia, which accounts for 80 % of all stroke cases, is caused by the obstruction of a cerebral blood vessel by atherosclerosis or embolization. The limited supply of O_2 and nutrients creates a supply-demand mismatch, which compromises neuronal function. Most often, cerebral ischemia is incomplete, the brain is partially hypoperfused. Falling cerebral blood flow (CBF) from the normal 50 ml/100 g/min value, below 10 ml/100 g/min, causes anaerob metabolism and the disruption of cell membrane transport, leading to subsequent neuronal death within minutes. In focal ischemia, adjacent to the core of the injury, residual blood flow persists, the local CBF ranging between 15-25 ml/100 g/min or 20-40 % relative to baseline [3, 4]. This narrow tissue band embracing the infarcted core has been known as the ischemic penumbra [4]. In contrast with the necrotic core, the penumbra consists of electrophysiologically inactive but viable and, most importantly, salvageable tissue [4-7], which places it in the center of ischemic neuroprotective therapy.

Under physiological conditions, the Na^+/K^+-ATPase creates Na^+- and K^+-gradients necessary for generating cellular resting potential, the regulation of cell volume and many other ion-fluxes through the plasma membrane. This pump consumes as much as two thirds of the whole cell's energy production, which makes it extremely vulnerable to ATP reduction. Under

ischemic conditions, the lack of O_2 and nutrients results in mitochondrial damage, and ATP depletion. Within minutes after the ischemic insult, the failure of Na^+/K^+-ATPase causes a rapid increase of intracellular $[Na^+]$ and extracellular $[K^+]$. In addition, the subsequent membrane depolarization activates voltage-gated Ca^{2+} channels (VGCCs), which enable Ca^{2+}-influx. Water follows Na^+ passively into the cell to cause cell swelling [8] (**Fig. 1**). Ca^{2+}-overload in neurons is implicated in irreversible neuronal damage. On the other hand, Ca^{2+} accumulation in vascular smooth muscle cells (VSMCs) leads to massive vasoconstriction, which exacerbates the ischemic injury. Moreover, elevating intracellular $[Ca^{2+}]$ in excitatory neurons causes uncontrolled glutamate release. At the same time, the re-uptake of glutamate is impaired due to the lack of ATP and the disrupted Na^+-gradient. Elevated glutamate level, from the basal 3-6 µM up to the excitotoxic 20 µM in the ischemic core region is sustained up to hours after the ischemic insult [2, 9]. Expression of astrocytic glutamate-transporters (glutamate-transporter 1, glutamate-aspartate transporter) is failed after ischemia, that is why the buffering role of these cells is also impaired [9]. Extreme extracellular glutamate concentration results in the uncontrolled activation of glutamate-receptors, especially ionotropic N-methyl-D-aspartate (NMDA), α-amino-3-hydroxy-5-methyl-4-isoxazolepropionic acid (AMPA) and kainite receptors in neurons. Through the activated receptors, excessive amount of Na^+ and Ca^{2+} enters the cells, which activates protein degradation cascades. In neurons, NMDA receptor activation is coupled with neuronal NO synthase (nNOS). Under ischemic conditions, NO interacts with superoxide to produce peroxynitrite. The interaction of peroxynitrite with cell membrane lipids, proteins and DNA cause lipid peroxidation, protein oxidation and DNA fragmentation [10]. Additionally, glutamate-overload and excessive Ca^{2+}-influx activate reactive oxygen species (ROS) production through mitochondrial dysfunction [8, 9] (**Fig. 1**).

Besides Ca^{2+} channels, there are Ca^{2+} pumps in the cell membrane (high affinity plasma membrane Ca^{2+} ATPase (PMCA), low affinity Na^+-Ca^{2+} exchanger (NCX)), extruding Ca^{2+} from the cell opposite its gradient. PMCA removes Ca^{2+} from the cell, coupled with H^+ uptake [11], but the lack of ATP causes failure of this ATPase. In addition, NCX transports Ca^{2+} with a 10 to 50-fold higher transporting capacity than PMCA, moving 3 Na^+ into the cell opposite 1 Ca^{2+} at rest, using the power of the electrochemical gradient of Na^+. Since NCX is an electrogenic transporter, alteration of the membrane potential, or elevated intracellular $[Na^+]$ can reverse the direction of the exchange, which increases intracellular $[Ca^{2+}]$ [12]. Deficiency of these Ca^{2+} pumps contributes to the ischemia-induced Ca^{2+} overload, as well (**Fig 1**).
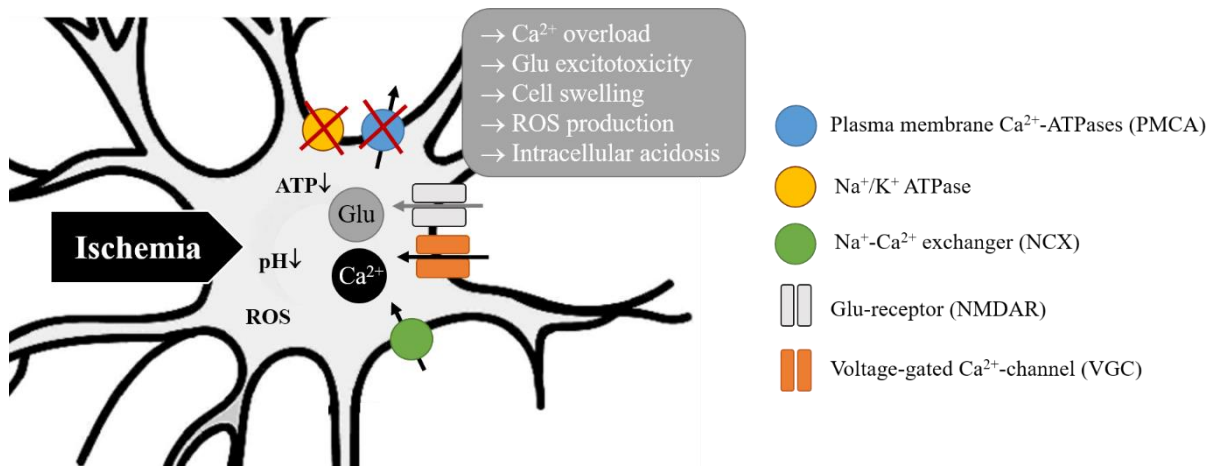
Figure 1. Proposed cellular mechanism of cellular damage in ischemic stroke include Ca^{2+} overload, glutamate excitotoxicity, cell swelling, ROS (reactive oxygen species) production and intracellular acidosis. The reduced availability of ATP leads to the failure of the Na^+/K^+ ATPase, the subsequent imbalance of intracellular ion homeostasis (rapid increase of intracellular $[Na^+]$ and extracellular $[K^+]$) and membrane depolarization. Excessive membrane depolarization causes VGCC (voltage-gated Ca^{2+}-channel) activation, contributing to intracellular Ca^{2+} overload (black arrows demonstrate Ca^{2+} influx), and glutamate excitotoxicity (grey arrow demonstrates glutamate influx). Water follows Na^+ and Ca^{2+} passively, to cause neuronal swelling. Failure of PMCA (plasma membrane Ca^{2+} ATPase) and NCX (Na^+-Ca^{2+} exchanger) Ca^{2+} pumps worsens ischemia induced Ca^{2+} overload. Glutamate excitotoxicity and excessive Ca^{2+} influx activate ROS production through mitochondrial dysfunction.

1.1.2. Pathophysiological impact of spreading depolarization

It is important to realize that the penumbra evolves dynamically in space and time [13]. After the onset of cerebral ischemia, spreading depolarization (SD) events evolve spontaneously from the border of the core and penumbra regions in clusters for several days after the ischemic insult [14, 15], and propagate across tissue at risk [13, 16-19]. In fact, recurrent SDs (rSDs), which are appreciated to arise at the inner penumbra, from minutes to days after the primary impact, have been understood as a principal mechanism of lesion progression in the acutely injured human brain [20, 21]. If the local concentration of extracellular K^+ and glutamate increases over-threshold, SD evolves and propagates via direct neuron-to-neuron gap junctions and volume transmission [22, 23]. SD is a synchronized wave of massive depolarization of cortical neurons and glia cells, propagating slowly (2-6 mm/min) across the cerebral grey matter [24]. This near complete depolarization is accompanied with local brain electrical silence, first identified as spreading depression of electrocorticographic activity by Arisitides Leão [14, 15]. SDs occur in hypoperfused nervous tissue due to metabolic supply demand mismatch [25], and in turn, exacerbate the ischemia-related metabolic burden [20]. The hallmark of SD is the negative shift of the DC (direct current) potential corresponding

9

to a rapid increase of extracellular $[K^+]$ (from 3-4 to 30-60 mM) and glutamate, and a rapid decrease of extracellular $[Na^+]$ (from 140-150 to 50-70 mM) and $[Ca^{2+}]$ (from 1-1.5 to 0.2-0.8 mM) [26]. Under ischemic conditions, the clearance of K^+ and glutamate by astrocytes is saturated, which sustains the depolarization and delays the repolarization from SD. **(Fig 2).**

Releasing metabolites and ions (K^+, lactate, ATP/ADP, and adenosine), the production of vasoactive substances (e.g., prostaglandins), and remarkable metabolic demand with SD events generate a hemodynamic response typical of the metabolic status of the tissue. In the optimally perfused, intact brain, the CBF response to SD consists of three subsequent elements: a brief transient hypoperfusion, a transient peak and late hyperemia, and a focal, long-lasting oligemia [27]. In contrast, in the injured brain (e. g. ischemic or hemorrhagic stroke, traumatic brain injury), vasoconstrictive elements of the CBF response dominate at the expense of hyperemia, which is instrumented by the release of vasoconstrictive substances. Depending on the severity of ischemia, a theoretical spectrum of the CBF response from reducing hyperemic component to spreading ischemia have been established [28] **(Fig 2)**.

Over the recent years, the opinion has been formulated that the pattern of SD recurrence should be considered as a biomarker of metabolic failure in neurointensive care [29], and SDs have been proposed as a therapeutic target in the management of acute brain injury, including ischemic stroke [30].
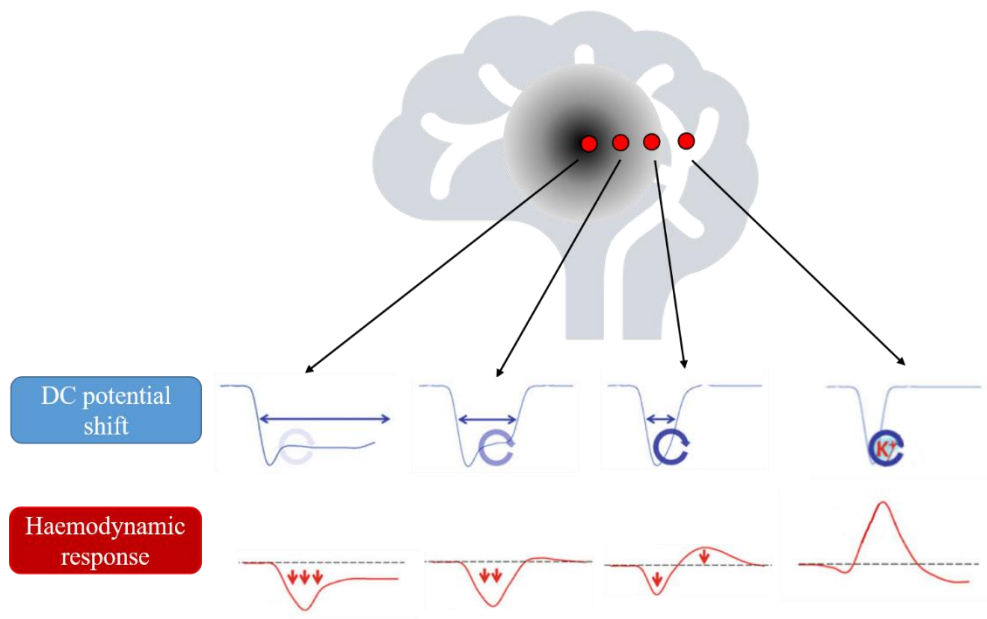
Figure 2. The conceptual spectrum of the DC potential shift (blue curves) and hemodynamic response (red curves) with spreading depolarization after a focal ischemic insult. Note that the local perfusion pressure reduces from penumbra (grey area) to the core region (black area). The longer the total depolarization time, the deeper the hypoperfusion is. Moreover, the clearance of K^+ by Na^+/K^+ ATPase is diminished in the core region (based on Hoffmann and Ayata, 2013 [31]).

1.1.3.   Mechanisms to cause cerebral ischemic tissue acidosis

The shortage of metabolic substrates and O_2, a condition that characterizes cerebral ischemia leads to metabolic acidosis. The limited availability of O_2 favors anaerobic glycolysis: pyruvate is reduced to lactate at the concomitant generation of a H^+, which causes lactic acidosis [32]. In turn, tissue pH after cerebral ischemia onset decreases following an inversely linear relationship with tissue lactate concentration [32-35]. In addition, tissue pCO_2 rises to 3-4 fold, which may also contribute to tissue acidosis [36] (**Fig 1**).

Even though astrocytes were initially thought to be a major source of acid production under cerebral ischemia [37, 38], this interpretation was later contended and compartmentation of H^+ was found to be negligible in the ischemic nervous tissue [35, 39]. Intra- and extracellular acidosis with SD acquired at tissue level also displayed corresponding kinetics [40], indicating that acidosis in the intra- and extracellular space must be approximately consistent in metabolically challenged tissue. Indeed, intra-, and extracellular pH in the ischemic nervous tissue probably equilibrates rapidly, because lactate newly produced in neurons and astrocytes is quickly released into the extracellular space as lactic acid via lactate/proton cotransport [41].

Although metabolic acidosis may therefore not be restricted to specific tissue compartments, the acidosis can be localized to distinct tissue regions, and the magnitude of the

pH shift is subject to the type or severity of the ischemic insult. For example, in a feline model of complete global forebrain ischemia, tissue pH fell to 6.2-6.6 units [36, 42]. Alternatively, in the rat incomplete global forebrain ischemia model achieved with the bilateral occlusion of the common carotid arteries (2-vessel occlusion, 2VO), pH 6.9-7.1 indicated relatively mild acidosis in the parietal cortex [40]. In focal cerebral ischemia, the degree of acidosis displays spatial variation, and particular values are typical for discrete tissue zones. As such, tissue pH in the ischemic core may become as low as pH 6.0, while tissue pH fluctuates around pH 6.5-6.9 in the peri-infarct penumbra, as estimated in the acute middle cerebral artery occlusion (MCAO) rodent model of focal ischemic stroke [43, 44].

Simultaneous with the negative shift of the DC potential, an extracellular pH-change is initiated starting with a short alkaline shift, which is followed by a longer lasting transient acidosis [45-47], and thus a decrease of tissue pH by around 0.3-0.5 pH units [40, 45]. The duration of the SD-related acid burden corresponds to SD duration lasting for a few minutes under ischemic penumbra conditions [48], which is increasingly longer in tissue zones undergoing more severe metabolic crisis [20, 49]. Moreover, the SD-related acid load is remarkably extended with aging in the ischemic nervous tissue, which may contribute to the age-related acceleration of ischemic lesion maturation [48, 50]. The SD-related acidosis has been understood to reflect lactate accumulation, which corresponds with the duration of the negative pH shift with SD, modulates transmembrane ion-transport, and determines the amplitude of pH-response [45]. Previous observations show that, lactate accumulation in the cortex during SD can be facilitated under ischemic conditions [47, 48]. Lactate, as a product of anaerobic glycolysis, plays an important role in neuronal metabolism and signaling. In case of an ischemic insult, lactate can be neuroprotective by increasing energy availability, but if rSDs are spreading across the ischemic cortex, extra lactate accumulation can deepen the metabolic crisis of the damaged tissue [51]. The duration and the magnitude of tissue acidosis influence the survival of neurons and glia cells. The acidosis associated with a single SD would probably not harm neurons, but rSDs in close succession reduce the tissue pH below 7.0 permanently [44, 52, 53]. This is of importance because the prolongation of acid exposure is understood to lower the threshold of acidosis-induced cell death [54]. Moreover, transient tissue acidosis associated with SD events superimposed on ischemia-related acidosis, deepen tissue pH in the penumbra near levels typical of the core **(Fig 3)**.
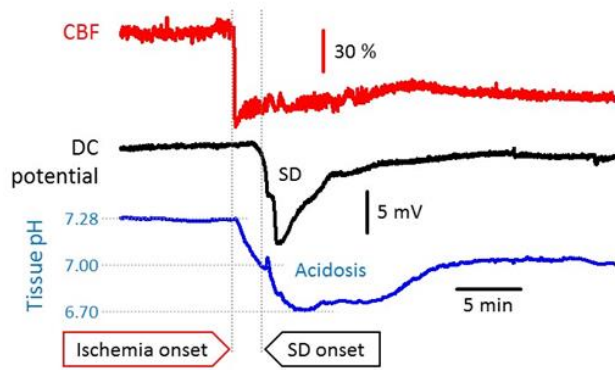
Figure 3. Representative traces demonstrate the association of tissue acidosis (blue) with ischemia onset (bilateral common carotid artery occlusion; red) and spreading depolarization (SD; black) in the rat parietal cortex. Tissue pH was measured with a pH-sensitive microelectrode implanted in the cortex, cerebral blood flow (CBF) was monitored with laser Doppler flowmetry, and the DC potential was acquired with an intracortical glass capillary microelectrode.

1.2. Ca^{2+}-channel blockade in the treatment of cerebral ischemia

1.2.1. Intracellular Ca^{2+} homeostasis in the nervous system

The 100 000-fold concentration gradient among the extracellular (1 mM) and cytosolic free (100 nM) Ca^{2+} concentration ($[Ca^{2+}]$) makes this ion a special second messenger, especially in the central nervous system [55]. The intracellular $[Ca^{2+}]$ can increase up to several μM during various cellular functions, like synaptic transmission in neurons or constriction in contractile cells. Because of the low Ca^{2+}-permeability of the cell membrane, highly selective ligand- and voltage-gated Ca^{2+}-channels regulate Ca^{2+}-transport, while in the cytosolic Ca^{2+}-binding proteins and intracellular stores sustain the level of free Ca^{2+} in physiological range in each cell type of the brain.

According to the opening mechanism, three major categories of Ca^{2+}-channels in the plasma membrane are differentiated: voltage-gated (VGCC), receptor-operated and store-operated Ca^{2+}-channels [12]. This thesis focuses on VGCCs, which are important regulators of depolarization-induced Ca^{2+}-entry along its electrochemical gradient causing local elevation of intracellular $[Ca^{2+}]$ [56]. There are two major types of VGCCs according to the rate of the activating voltage-changes: high and low voltage-activated channels (HVA, LVA). Among the HVA channels several subtypes have been identified based on their pharmacological responsiveness; L-type channels are dihydropyridine-sensitive; P/Q-type channels are inhibited by ω-agatoxin, N-type channels can be blocked by ω-conotoxin, R-type channels can be inhibited by SNX-482 tarantula venom, and T-type channels are sensitive to cadmium [56]. VGCCs are located on neurons, vascular and skeletal muscle fibres or cardiac myocytes [57]. These channels regulate neuronal functions, like gene transcription, synaptic transmission, or activation of Ca^{2+}-dependent enzymes in neurons and mediate the

excitation-contraction coupling and the repetitive firing of cardiac myocytes and VSMC contraction and growth [12, 57].

1.2.2. The mechanism of action of the voltage-gated Ca^{2+} channel-blocker nimodipine

In the last four decades, numerous animal experiments have indicated that administration of VGCC blockers is effective in the treatment of cerebral ischemia, at the same time, it is hard to translate these data into clinical trials. One of the most potent blockers of VGCCs is nimodipine, with relatively selective pharmacological effect on cerebral vessels and neurons. This dihydropyridine derivative inhibits Ca^{2+}-influx through vascular and neuronal L-type VGCCs, causing vasodilation and neuroprotection in the central nervous system. Due to its lipophilicity, it can cross the blood-brain barrier (BBB), augmenting its central effect [58].

About four decades ago Steen et al. (1983) found that nimodipine increased CBF after complete cerebral ischemia in dogs [59]. In another experiment, nimodipine administered intravenously (2 µg/kg/min) 1, 4 or 6 hours after the ischemic insult, improved neurological outcome and reduced the infarction volume after acute focal cerebral ischemia created by the occlusion of middle cerebral artery of rats [60]. The blockade of L-type VGCCs by nimodipine reduced the elevation of intracellular $[Ca^{2+}]$ and shortened the duration of membrane depolarization in the oxygen-glucose deprivation model of stroke in rat brain slices [61]. This finding supports the role of L-type VGCCs in the early phase of ischemic cell damage and makes nimodipine a possible candidate for ischemic stroke therapy. Under ischemic conditions, nimodipine moderately impedes SD events [62], efficiently improves the hyperemic component of SD [63, 64] and converts spreading ischemia to a hyperemic response [65, 66].

At present, in clinical practice, nimodipine is the only drug available to reduce the risk of delayed cerebral ischemia and subsequent delayed ischemic neurological deficit, which are the major causes of death and disability in patients with subarachnoid hemorrhage (SAH) [67]. Although its efficacy in SAH patients has been proven, the beneficial effects of nimodipine remain inconclusive in patients suffering from cerebral ischemia [68]. Under ischemic conditions, cerebral autoregulation may be impaired. For this reason, mean arterial blood pressure (MABP) must be monitored closely in patients suffering from ischemic stroke: cerebral perfusion pressure may decrease together with lowering blood pressure, which is accompanied by decreasing CBF due to impaired autoregulation. Although it is relatively selective to cerebrovascular VGCCs, nimodipine lowers MABP in a dose-dependent way [69].

That is why, during the therapy of stroke patients with normo- or hypotension, the hypotensive effect of VGCC blockers should be avoided.
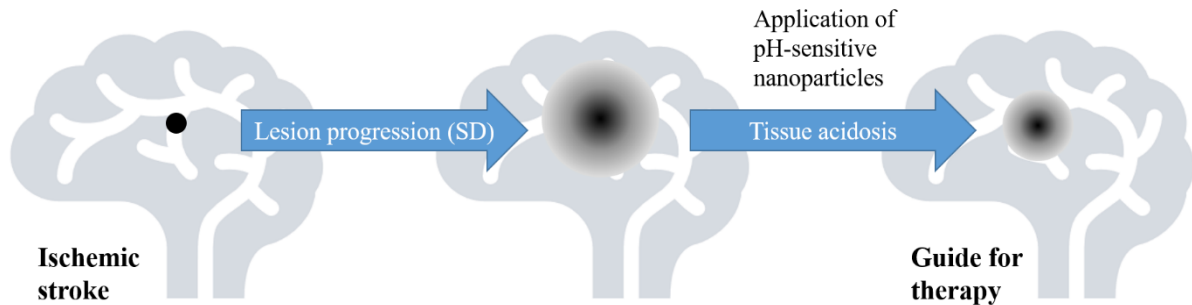
1.3. Cerebral tissue acidosis in stroke therapy and nanomedicine

Brain imaging (computer tomography – CT, and magnetic resonance imaging – MRI) is a first step in the diagnosis of stroke. Beyond the primary assessment of the nature (i.e., ischemic, or hemorrhagic), location, and volume of the injury of cerebrovascular origin, MRI, and positron emission tomography (PET) techniques have been central to identify the ischemic penumbra, prognosticate its evolution, aid personalized therapeutic decision making, and confirm the fate of the penumbra tissue after treatment [7, 70]. The reliable differentiation of the ischemic penumbra from the infarction or benign oligemic regions is, therefore, critical, and establishes the need to invent and refine applicable imaging tools [5]. The most recent developments in this field suggest that tissue acidosis can be used to distinguish penumbra tissue from the ischemic core with confidence, and the inclusion of pH imaging among imaging modalities used in stroke diagnostics has been recommended to bring informed decisions on patient care [7].

Obviously, the ischemic penumbra forms the central target of stroke therapy. Although recanalization is clearly intended to reperfuse and ideally save the ischemic penumbra, the delivery of pharmacological agents selectively to the penumbra zone is problematic and remains a field for exploration. Next to narrow therapeutic time-windows, obvious difficulties hamper drug delivery to the ischemic territory, including the vascular occlusion blocking the direct vascular route of drug delivery, and the selective permeability of the BBB if it remains intact. Yet, the residual blood flow typical of the ischemic penumbra may be sufficient in case the efficacy of drug delivery is amplified with specific drug carrier and drug release systems that (i) can cross the intact BBB, (ii) respond to the ischemic environment, and (iii) increase the local concentration of the therapeutic agent.

Since nanomaterials have great potential of controlled and sustained drug release as well as biocompatibility and lower toxicity to human tissues, nanomedicine is having increasingly more significant impact in stroke therapy. Nanoparticles fall under structurally heterogenic groups of 1-1000 nm particles, they can potentiate the penetration of agents into the brain by prolonging their circulation time and promoting the transport of drugs through biological membranes and the BBB [71]. Intensive research in nanomaterial sciences has shown that different properties (shape, size, composition, surface charge, hydrophilicity, rigidity, and conductivity) of nanoparticles are modified effectively. Drugs can be released temporally or

regionally by various internal (pH, redox, specific biomolecules, or enzymes), and external (temperature, electromagnetic radiation, ultrasound) stimuli, targeting the drug to the injured region **(Fig. 4)**.

Figure 4. Application of pH-sensitive nanoparticles appears to be a feasible solution for neuroprotection in ischemic stroke therapy. Tissue acidosis linked to cerebral ischemia and spreading depolarization (SD) can be utilized as a trigger for drug release.

Intriguingly, cancer therapy has already identified low pH typical of the tumor environment to direct anticancer drug delivery selectively to a tumor to enrich the tumor tissue with anticancer agents [72, 73]. An analogous approach is thought to open up new possibilities in ischemic stroke therapy [74, 75], and may advance the management of ischemic stroke in the future.

2. Experimental hypothesis and aims

Based on the above, we **hypothesized,** that:

- Nanoparticles are suitable for targeting drug release to the ischemic region in the nervous tissue.
  - Tissue acidosis caused by ischemia or SD occurrence is a condition that can be harnessed to initiate drug release in the injured nervous tissue.
- Application of nimodipine is suitable for testing a novel pH-sensitive nanocarrier system in an *in vivo* global cerebral ischemia model.
  - Nimodipine is expected to re-establish neurovascular coupling that is injured under ischemia.
  - Nimodipine administered with nanoparticles is anticipated to exert vasodilator and neuroprotective effect against SD, propagating over the ischemic penumbra.

According to our hypothesis, our **aim** was:

- To investigate the impact of topically administered nimodipine in solution in the intact and ischemic brain;
- To design and test a novel treatment strategy resting on pH-sensitive nanoparticles carrying nimodipine, to be administered topically in our *in vivo* global cerebral ischemia model.

3. Materials and methods

3.1. Surgical procedures

All experiments were approved by the National Food Chain Safety and Animal Health Directorate of Csongrád County, Hungary. The procedures conformed to the guidelines of the Scientific Committee of Animal Experimentation of the Hungarian Academy of Sciences (updated Law and Regulations on Animal Protection: 40/2013. (II. 14.) Gov. of Hungary), following the EU Directive 2010/63/EU on the protection of animals used for scientific purposes and reported in compliance with the ARRIVE guidelines.

Two sets of experiments are presented in this thesis. In *Experimental Project I*, nimodipine was applied in solution. In *Experimental Project II*, nimodipine was associated with pH-sensitive nanoparticles in suspension.

Young adult, male Sprague-Dawley rats (Charles River Laboratories) were used in the projects. Animals were housed under a normal 12/12 h light/dark cycle and at constant temperature (23 °C). Standard rodent chow and drinking water were supplied *ad libitum*. On the day of experiments, animals were anesthetized with isoflurane (1.5-2 % in $N_2O:O_2$ 70 %:30 %) and allowed to breathe spontaneously through a head mask. In *Experimental Project I*, isoflurane was substituted by α-chloralose (dissolved in saline at a concentration of 7 mg/ml; administered as a bolus injection of 50 mg/kg for initiation, and then 30 mg/kg/h for maintenance, intraperitoneally) for the period of actual data acquisition. In *Experimental Project II*, isoflurane anesthesia was sustained throughout the experimental protocol. Body temperature was maintained at 37±0.5 °C by using a servo-regulated heating pad, feedback-controlled by a flexible rectal probe (Harvard Apparatus, Holliston, MA, U.S.A.). Atropine (0.1 %, 0.05 ml) was administered intramuscularly shortly before the surgical procedures to avoid the production of airway mucus. Lidocain (1 %) was administered topically before opening each tissue layer. The left femoral artery was cannulated to monitor MABP continuously, and to collect samples for arterial blood gas analysis. Samples for blood gas analysis were taken prior to the start of the experimental protocol (physiological condition) and shortly after the evolution of the last SD event in a train (ischemic condition) (Epoc Reader, Epocal, Ottawa, Canada). The depth of anesthesia was regularly checked and controlled with the aid of MABP. Both common carotid arteries were carefully separated from the surrounding tissue and an occluder was looped around each vessel for later induction of acute, incomplete, global forebrain ischemia.

The head of the rats was fixed into a stereotactic frame (Stoelting Co., Wood Dale, IL, USA) and the skin above the skull and temporal muscle was retracted from the underlying right parietal and temporal bones. Two cranial windows (~3x3 mm) were prepared on the right parietal bone (3 mm caudal and 5 mm lateral, or 7 mm caudal and 5 mm lateral from bregma; in *Experimental Project I* or *II*, respectively) with a high precision dental drill (Technobox, Bien Air 810, Switzerland; or ProLab Basic, Bien-Air Dental SA, Bienne, Switzerland) under saline cooling. The cortical surface was exposed by the careful retraction of the dura mater in each cranial window. The rostral window was later used for data acquisition (i.e., reference electrode recording local field potential (LFP) filtered in DC mode, and an adjacent Laser-Doppler probe for electrophysiology and CBF measurement in both experimental projects, and a pH sensitive microelectrode for extracellular pH measurement in *Experimental Project II*) and topical drug administration, while the caudal window served SD elicitation **(Fig 5)**. The craniotomies were regularly irrigated with artificial cerebrospinal fluid (aCSF; mM concentrations: 126.6 NaCl, 3 KCl, 1.5 $CaCl_2$, 1.2 $MgCl_2$, 24.5 $NaHCO_3$, 6.7 urea, 3.7 glucose bubbled with 95 % O_2 and 5 % CO_2 to achieve a constant pH of 7.4). In *Experimental Project I,* experiments were terminated at the end of the experimental protocol by the overdose of the anesthetic agent. In *Experimental Project II,* the animals were sacrificed under deep anesthesia with transcardiac perfusion.
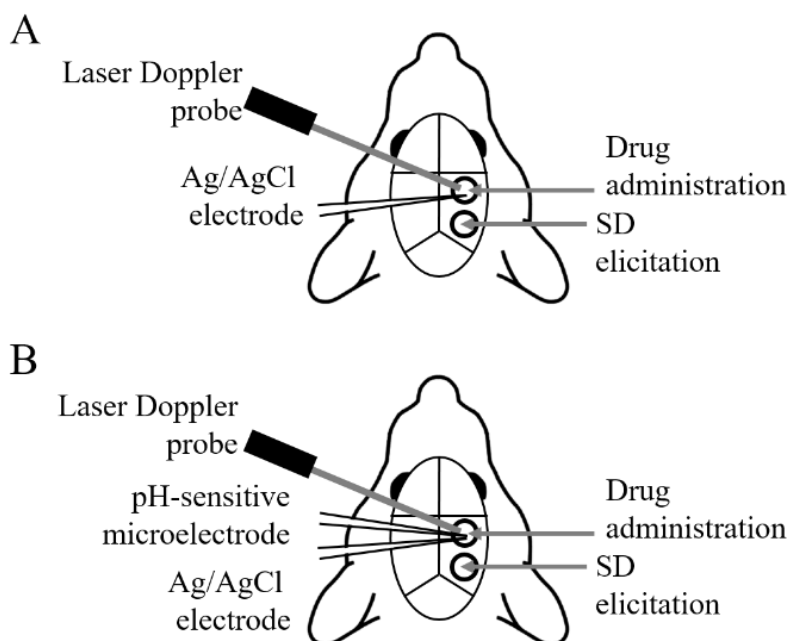
Figure 5. The preparation in *Experimental Project I* (**Panel A**) and *II* (**Panel B**). The rostral window was used for data acquisition (i.e., Ag/AgCl electrode recording of local field potential filtered in DC mode, Laser-Doppler probe for cerebral blood flow measurement, pH sensitive microelectrode for extracellular pH measurement) and topical drug administration, while the caudal window served spreading depolarization (SD) elicitation.

3.1. Recording of electrophysiological variables and extracellular pH

A saline-filled glass capillary electrode (20 µm outer tip diameter) was inserted 700-1000 µm deep into the cerebral cortex at the rostral window for the synchronous recording of the LFP and the slow cortical or DC potential and was also used as reference for the pH-sensitive electrode. An Ag/AgCl electrode inserted subcutaneously in the neck served as common ground in both experimental projects.

In *Experimental Project I*, the electrophysiological signals were recorded via a high input impedance pre-amplifier (NL102GH, NeuroLog System, Digitimer Ltd., United Kingdom), connected to a differential amplifier (NL106, NeuroLog System, Digitimer Ltd., United Kingdom) with associated filter and conditioner systems (NL125, NL530, NeuroLog System, Digitimer Ltd., United Kingdom). Potential line frequency noise (50 Hz) was removed by a high-quality noise eliminator (HumBug, Quest Scientific Instruments Inc., Canada) without any signal attenuation. Analogue to digital conversion was performed by a dedicated analog-to-digital converter card (NI USB-6008/6009, National Instruments, Austin, Texas, USA) controlled through a custom-made software, written in LabView (National Instruments, Austin, Texas, USA).

In *Experimental Project II*, ion-sensitive microelectrodes were prepared according to Voipio and Kaila (1993) [76]. Glass capillary microelectrode tips (outer diameter: 10-12 µm) were filled with a liquid H^+-ion exchanger, and the shank of the microelectrode was backfilled with 150 mM NaC1 + 40 mM HEPES (4-(2-hydroxyethyl)-1-piperazineethanesulfonic acid) + 20 mM NaOH. Each pH-sensitive microelectrode was calibrated in standard solutions of known pH (pH 8.05, 7.02, 6.2; calibration solution containing 150 mM NaCl + 40 mM HEPES). Microelectrodes were connected to a custom-made dual-channel high input impedance electrometer (including AD549LH, Analog Devices, Norwood, MA, USA) via Ag/AgCl leads. The voltage signal recorded by the reference electrode was subtracted from that of the pH-sensitive microelectrode by dedicated differential amplifiers and associated filter modules (NL106 and NL125, NeuroLog System, Digitimer Ltd, United Kingdom), which yielded potential variations related to changes in extracellular $[H^+]$. The recorded signals were then forwarded to an analog-to-digital converter (MP 150, Biopac Systems, Inc). In *Experimental Project II*, electric signals were continuously acquired at a sampling frequency of 1 kHz. Extracellular pH changes were expressed in mV to be translated into pH units offline, using least squares linear regression. The tips of the two electrodes were implanted as near as possible.

3.2. Monitoring of local cerebral blood flow

Laser Doppler flowmetry (LDF) was used to record changes in local CBF in response to SD events in both experimental projects, and somatosensory (whisker) stimulation in *Experimental Project I*. A laser Doppler needle probe (Probe 403 connected to PeriFlux 5000; Perimed AB, Sweden) was positioned above the barrel cortex. The probe was positioned right above the cortical surface at the penetration site of the glass capillary electrodes with a micromanipulator, avoiding any large pial vessels. In *Experimental Project I*, the ideal position of the LDF probe was identified prior to the actual experimental protocol: the probe was positioned over the region where the amplitude of functional hyperemia in response to whisker stimulation proved to be the greatest. In both experimental projects, the signal was digitized and acquired, together with the DC potential, LFP and pH signals essentially as described above (MP 150 and AcqKnowledge 4.2.0, Biopac Systems, Inc. USA). In *Experimental Project II*, the completed preparation was enclosed in a Faraday cage.

3.3. Pharmacological treatment

Animal selection for treatment was random by alternating treatment as the experimental work proceeded. In *Experimental Project I*, the rostral cranial window was incubated with nimodipine (Sigma-Aldrich, 100 μM in 0.1 % DMSO (dimethyl-sulfoxide) in aCSF; n=12) following 5 min baseline recording. The drug solution was refreshed every 10 min to maintain efficacy until the termination of each experiment. In other rats, rinsing the cranial window with vehicle served as control for pharmacological treatment (n=17).

In *Experimental Project II*, chitosan nanoparticle suspension – either loaded with nimodipine, or devoid of the pharmacon (i.e., vehicle) – was prepared in aCSF according to Janovák et al. (2018) [74]. The nanoparticle suspension was expected to release nimodipine in response to a pH shift from physiological (~pH 7.35) to acidic (~pH 6.75) [74]. The rostral cranial window was incubated with the nanoparticle suspension including nimodipine (100 μM; n=10) or vehicle (n=8). Suspensions were refreshed every 10 minutes until the termination of the experiment.

3.4. Experimental protocol

In *Experimental Project I*, after drug incubation for 30 min, both common carotid arteries were permanently occluded by pulling on the occluder lines until resistance was felt, and then the occluders were secured in place (n=14). Successful 2VO was confirmed by an immediate, sharp drop of the LDF-signal displayed live. Rats with no occlusion served as

control for 2VO (i.e., intact, n=15). Fifteen minutes after 2VO onset, whisker stimulation involving the entire left whisker pad was performed mechanically. Stimulation frequency was set at 2-3 Hz, each stimulation lasting for 25 s. The stimulation was repeated 4 times with 2 min intermissions. Subsequently, three SD events were triggered by placing a 1 M KCl-soaked tiny cotton ball in the caudal craniotomy. The cotton ball was removed, and the craniotomy rinsed with aCSF after each successful SD elicitation, to allow the evolution of a single SD in response to each triggering. SDs were provoked at an inter-SD interval of at least 15 min. Considering the combination of 2VO and pharmacological manipulations, 4 experimental groups were established (**Fig. 6A**).

In *Experimental Project II*, after a baseline period of 10 minutes, the nanoparticle suspension was washed to the brain surface. Ten minutes later, incomplete, global forebrain ischemia was induced by 2VO, as described above. Fifteen minutes after 2VO onset, three SD events were evoked by the topical administration of 1 M KCl. According to the pharmacological treatment, 2 experimental groups were formed (**Fig. 6B**).
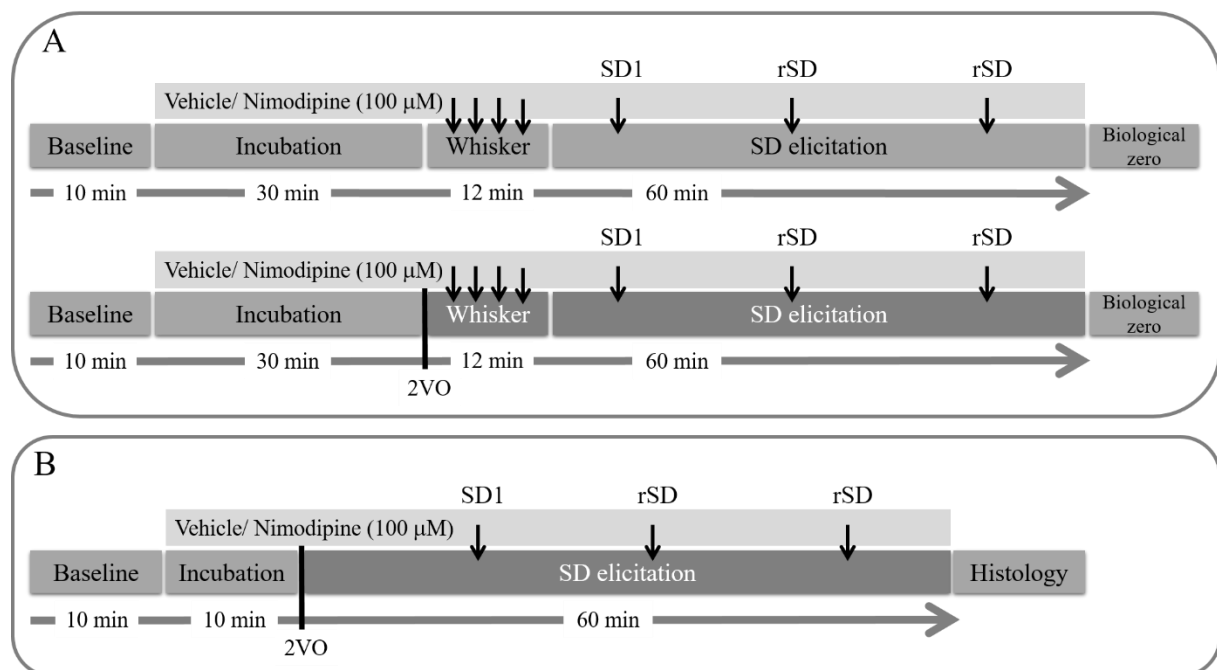
Figure 6. Timelines of the protocols implemented in *Experimental Project I* (**Panel A**) and *II* (**Panel B**). Abbreviations: 2VO, permanent, bilateral occlusion of the common carotid arteries ("two-vessel occlusion"); SD, spreading depolarization; SD1, first spreading depolarization in a train; rSD, recurrent spreading depolarization.

3.5. Histology

In *Experimental Project II*, 1-1.5 h after ischemia induction, animals (n=16) were transcardially perfused in deep anesthesia with physiological saline followed by 4 % paraformaldehyde (PFA). The brains were removed and postfixed overnight in 4 % PFA. Coronal forebrain sections of 20 μm thickness were cut with a vibratome (Leica VT 1000S; Leica Microsystems, Wetzlar, Germany). Microglia were labelled with Iba1 (ionized calcium binding adaptor molecule 1; rabbit anti-Iba-1 primary antibody, 1:3000, 019-19741, Fujifilm Wako Chemicals Europe GmbH, Neuss, Germany) to explore whether the experimental procedures or the topical application of the nanoparticle suspension by itself induced microglial activation. To estimate neuronal loss due to SD, and neuroprotection offered by nimodipine, neurons in free floating slices were labelled for the marker NeuN (neuronal nuclei) with immunohistochemistry (rabbit anti-NeuN primary antibody; 1:300, ab177487, AbCam, Cambridge, UK). Endogenous peroxidase activity was blocked with 5 % H_2O_2, the nonspecific protein binding sites were blocked with 5 % normal goat serum (Merck, Kenilworth, New Jersey, USA) and the slices were permeabilized with Triton X-100 (Merck, Kenilworth, New Jersey, USA). Color reaction was developed with a Polink-2 Plus HRP Detection Kit for rabbit primary antibody with DAB (diaminobenzidine) chromogen (GBI Labs, Bothell, WA, USA). The slices were mounted on microscopic slides with Eukit® (Merck, Kenilworth, New Jersey, USA) and digitally recorded with a microscope slide scanner (Zeiss Mirax Midi Slide Scanner, Carl Zeiss MicroImaging GmbH, Jena, Germany) operated by a CaseViewer software (3D Histech Ltd., Budapest, Hungary). The slides were evaluated with ImageJ (Wayne Rasband, NIH) software.

Microglial activation was characterized with a ramification index calculated according to previously established principles [77, 78]. In each animal, 3 coronal brain slices were selected for the analysis. In each slice, 3 photomicrographs were taken at 20x magnification along the depth of the parietal cortex in both hemispheres. A 126x126 μm grid was placed on each of the 9 photomicrographs. Microglial branches/grid intersections (B) as well as microglial cell bodies within the grid (CBD) were counted manually with the Cell Counter plugin of ImageJ. The ramification index (RI) was calculated according to the following formula: $RI=B^2/CBD$. Since activated microglia are characterized by the retraction of their processes (i.e., amoeboid shape), high ramification index corresponds to the resting state of microglia, while low ramification index reflects microglial activation.

Neuronal loss in the ipsi- and contralateral parietal cortex was characterized by the estimation of NeuN positive immunolabeling in a cortical area of a standard size. In each

animal, 3 coronal brain slices were selected for the analysis. In each slice, 2 photomicrographs were taken at 5x magnification along the depth of the parietal cortex in both hemispheres. After masking binary images in ImageJ, the relative surface covered by NeuN-positive cell bodies was expressed.

3.6. Data processing and analysis

All variables (i.e., DC potential, LDF signal, MABP and extracellular pH) were simultaneously acquired, displayed live, stored, and analyzed using a personal computer equipped with a custom-made software in LabView in *Experimental Project I* (National Instruments, Austin, Texas, USA) or with a dedicated software in *Experimental Project II* (AcqKnowledge 4.2 for MP150, Biopac Systems, Inc., USA). Raw LDF recordings were down sampled to 1 Hz and then expressed relative to baseline by using the average CBF value of the first 5 minutes (100 %) and the recorded biological zero obtained after terminating each experiment (0 %) as reference points. In *Experimental Project I*, evoked field potentials (EFP) during whisker stimulation were analyzed in the original LFP recordings acquired at 2000 Hz, while raw DC recordings were also down sampled to 1 Hz in both experimental projects. Offline analysis was assisted by the inbuilt instructions of the software AcqKnowledge 4.2 for MP 150 (Biopac Systems, Inc., Goleta, USA). In *Experimental Project II*, full data analysis was conducted for animals whose cerebrocortical tissue pH varied in the physiological range prior to the application of nanoparticles (n=9).

In *Experimental Project I*, in case of whisker stimulation, the peak amplitude of evoked potentials was assessed to reveal drug effect, if any. The efficacy of hyperemia was characterized by measuring the maximum amplitude of the CBF response (mean of 15 s at the plateau of the hyperemia).

For SD events, data were evaluated separately for the first SD (SD1), and rSD events, because of the known differences in the kinetics of the SD-associated CBF response [79]. SD-associated hyperemia was characterized by; (i) the amplitude of the peak hyperemia, (ii) the duration of peak hyperemia at half amplitude and (iii) the magnitude (i.e., area under the curve, AUC) of the hyperemic response. SDs on the DC potential trace were analyzed by the following parameters: (i) amplitude of depolarization, (ii) duration of depolarization at half amplitude, (iii) AUC of the negative DC shift, (iv) rate of depolarization and (v) repolarization. SD events, which exceeded the selection criteria for the time at half amplitude (>200 seconds) were excluded from the analysis. In *Experimental Project II*, extracellular pH signal indicative

of SD was characterized by (i) amplitude of the transient acidosis, (ii) duration at half amplitude, (iii) AUC of the pH response, and (iv) rate of acidosis and (v) recovery.

Blinding data analysis was intended by assigning codes to files and recordings, which do not reveal the experimental condition (i.e., date of the experiment). All recordings were first screened for events suitable for comprehensive analysis. Data are given as mean ± standard deviation (stdev). The results were statistically analyzed with the software SPSS (IBM SPSS Statistics for Windows, Version 22.0, IBM Corp., USA). A repeated measure, a one-way or a two-way analysis of variance (ANOVA) model was used, dependent on the type of data set. Tukey, Games-Howell, or Fisher post hoc test was used for group comparisons, whenever applicable. Levels of significance were defined as $p < 0.05$* and $p < 0.01$**. Non-parametric data were statistically evaluated with a Pearson Chi-Square Test for Association. All relevant statistical methods are given in each figure legend.

4. Results

4.1. Physiological variables

Physiological variables (arterial blood pH, partial arterial pressure of O_2 and CO_2, MABP) are presented in **Table 1**. Statistical analysis did not reveal any significant ischemia- or treatment-related difference across experimental groups. Variables were in the physiological range prior to the initiation of the experimental protocol ($pO_2=144.4\pm24.4$ mmHg, $pCO_2=39.8\pm9.9$ mmHg, blood pH=7.36 ± 0.03), with a shift to higher pCO_2 and lower pH values 45-50 min after ischemia onset ($pO_2=128.0\pm29.3$ mmHg, $pCO_2=48.7\pm14.2$ mmHg, blood pH=7.28 ± 0.06).

Table 1. Physiological variables and number of animals included in each experimental group. Data are given as mean±stdev. Abbreviations: Exp. Project: Experimental Project, Pharm. treatm.: pharmacological treatment, Isch. induction: ischemia induction, Art. pCO_2: arterial partial pressure of CO_2, Art. pO_2: arterial partial pressure of O_2, Nimo: nimodipine, NP: nanoparticle, 2VO, permanent, bilateral occlusion of the common carotid arteries ("two-vessel occlusion"); MABP, mean arterial blood pressure.

Exp. Project	Pharm. treatm.	Isch. induction	n	Body weight (g)	Art. blood pH	Art. pO_2 (mmHg)	Art. pCO_2 (mmHg)	MABP prior to drug/ vehicle admin. (mmHg)	MABP after drug/ vehicle admin. (mmHg)
Exp. Project I	Vehicle	Intact	9	335±32	7.33±0.07	140.4±29.6	47.4±11.4	92±14	100±22
		2VO	8	326±48	7.33±0.03	127.0±32.8	39.9±6.3	100±1	102±8
	Nimo	Intact	6	331±31	7.39±0.06	103.4±16.1	44.8±8.1	103±18	106±15
		2VO	6	313±25	7.30±0.05	99.8±4.4	56.2±11.2	89±12	92±15
Exp. Project II	NP only	2VO	8	335±21	7.37±0.03	158.9±21.4	34.8±11.2	86±5	95±10
	Nimo + NP	2VO	10	342±48	7.35±0.03	131.6±20.5	44.0±7.3	89±11	88±10

4.2. Baseline variations of cerebral blood flow, mean arterial blood pressure and tissue pH, and the evidence for drug release from nanoparticles

Typical, original recordings of the DC potential and CBF variations over the full experimental protocol of *Experimental Project I* are shown in **Figure 7**. Variation of baseline CBF was assessed at selected time points of the experimental protocol, to evaluate the impact of pharmacological treatments (**Fig. 8**).
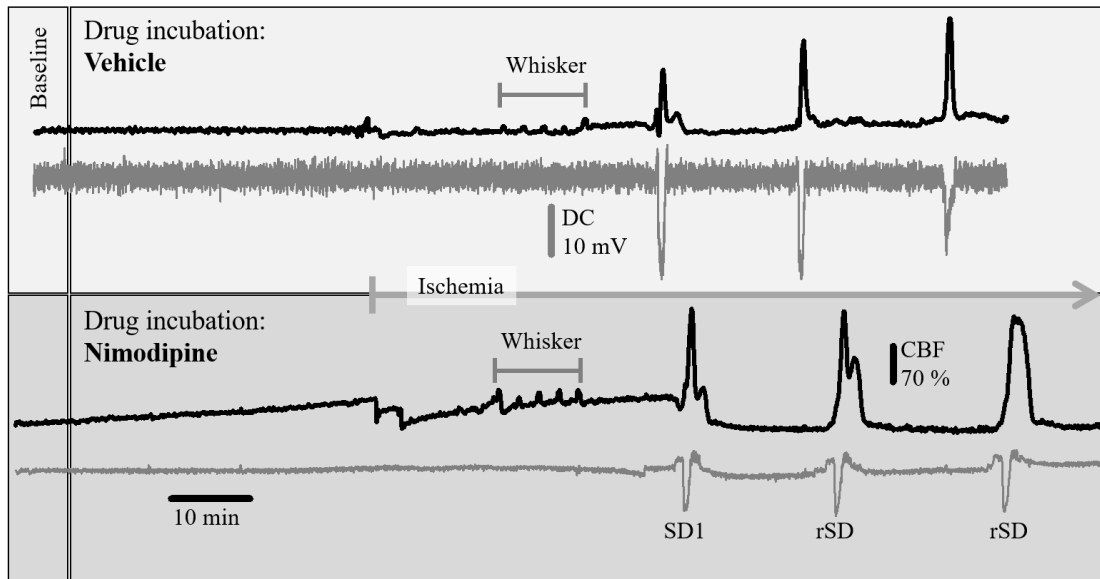
Figure 7. Representative direct current (DC) potential and cerebral blood flow (CBF) traces of the full experimental protocol including common carotid artery occlusion (2VO) under vehicle (upper box) or nimodipine (lower box) treatment. The traces were downsampled to 1 Hz frequency, and the CBF traces were smoothed by median filtering for 6 data points. Note that nimodipine gradually elevated baseline perfusion, increased the amplitude of functional hyperemia to whisker stimulation, and enlarged hyperemia in response to the first (SD1) and recurrent spreading depolarizations (rSDs). Also, nimodipine reduced SD amplitude. Note also the strikingly different size of the CBF response to whisker stimulation and SD within the same preparation.

In *Experimental Project I*, ischemia induction caused a marked reduction of CBF (to 53 ± 23 %), which stabilized in the vehicle-treated group at 74 ± 11 % prior to SD1, and at 67 ± 15 % prior to rSDs **(Fig. 8B, C and D)**. The occurrence of SD produced long-lasting oligemia, the final element of the CBF response to SD, which was apparent between SD events in the intact groups, as well. Nimodipine treatment increased baseline CBF significantly by the time of ischemia induction with respect to the pre-treatment CBF level (131 ± 43 vs. 104 ± 12 %, nimodipine vs. vehicle) **(Fig. 8A)**. Further, nimodipine counteracted CBF reduction due to 2VO (CBF shift from baseline: 22 ± 11 vs. -26 ± 11 pp., nimodipine vs. vehicle), and prevented the evolution of post-SD oligemia (CBF shift from baseline: 11 ± 24 vs. -30 ± 12 pp., nimodipine vs. vehicle in the intact group) **(Fig. 8B, C and D)**.

In *Experimental Project II*, CBF elevation was taken as a reliable read-out of the efficacy of nimodipine treatment and was expected to confirm drug release from nanoparticles. In contrast with *Experimental Project I*, local CBF remained level during the incubation period prior to ischemia onset (99.2 ± 2.6 vs. 99.9 ± 3.0 %, 30 min after vs. before the application of nimodipine associated to nanoparticles) **(Fig. 8A)** in the face of invariable tissue pH (pH 7.29 ± 0.22 vs. 7.28 ± 0.18, 30 min after vs. before the application of nimodipine associated to

nanoparticles) (($\mathbf{a}$) and ($\mathbf{b}$) in **Fig. 8E**). Ischemia induction produced a sharp drop of CBF to 29.4±10.2 %, and an acidic tissue pH shift to 7.06±0.30 (($\mathbf{c}$) in **Fig. 8E**). From this point on, CBF sampled prior to SD events increased in the nimodipine group, and was higher than in the vehicle group, particularly prior to rSDs (47.8±23.7 vs. 29.3±6.96 %, nimodipine vs. vehicle) (($\mathbf{f}$) in **Fig. 8E**), which were triggered subsequent to the transient reduction of tissue pH to 6.71±0.29 with SD1 (($\mathbf{e}$) in **Fig. 8E**). At the same time, the expected release of nimodipine from the nanoparticles (($\mathbf{d}$) in **Fig. 8E**) did not exert any discernible impact on MABP (e.g., 96.7±14.3 vs. 92.0±10.9 mmHg, nimodipine vs. vehicle, after ischemia induction – and thus the initiation of drug release).
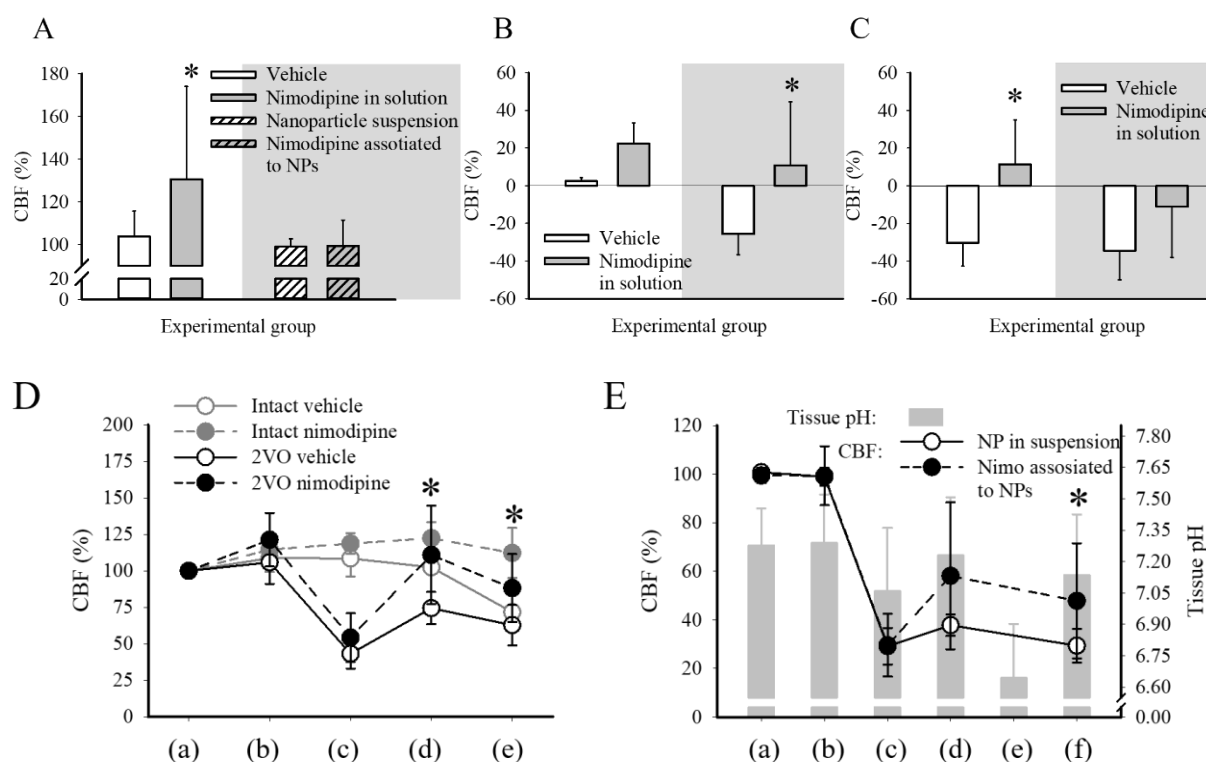
Figure 8. Variation of baseline cerebral blood flow (CBF, i.e., in between stimulations) with respect to pharmacological treatments.

  A) CBF baseline after 30 min of drug incubation, prior to the induction of ischemia in *Experimental Project I* and *II*. The intact group and the group of animals later undergoing bilateral common carotid artery occlusion (2VO) are merged, because they received identical handling until this point of the experimental protocol. Bars in front of white background represent *Experimental Project I*, while the bars in front of dark gray background stand for *Experimental Project II*. **B)** CBF before the induction of the first SD (SD1) in *Experimental Project I*. Data are expressed as change with respect to the corresponding baseline. **C)** CBF before the induction of recurrent SD events (rSD) in *Experimental Project I*. Note, that nimodipine significantly elevated baseline perfusion in each selected point of the experimental protocol. In panel B and C, bars in front of white background represent the intact condition, while the bars in front of dark gray background stand for bilateral common carotid artery occlusion (2VO).

  D) Variation of baseline cerebral blood flow (CBF) with respect to pharmacological treatment at selected points of *Experimental Project I*. Selected points of the experimental protocol: **(a)** before treatment initiation; **(b)** after treatment initiation; **(c)** minimum after ischemia induction; **(d)** prior to the first spreading depolarization (SD1); **(e)** prior to recurrent SD (rSD) events. **E)** CBF variation and tissue pH at selected points of *Experimental Project II*. Selected points of the experimental protocol: **(a)** before treatment initiation; **(b)** after treatment initiation; **(c)** minimum after ischemia induction; **(d)** prior to the first spreading depolarization (SD1); **(e)** pH minimum with SD1; **(f)** prior to recurrent SD (rSD) events. Note that CBF becomes significantly higher in the nimodipine group compared to the vehicle group following the tissue pH drop with ischemia induction. Data are given as mean±stdev. Statistical analysis relied on one-way ANOVA paradigm. The level of significance was defined as $p < 0.05$* vs. vehicle.

4.3. The impact of nimodipine on neurovascular coupling

The impact of nimodipine (in solution) on neurovascular coupling under intact and ischemic conditions was measured in *Experimental Project I*. For the estimation of drug effect on physiological neurovascular coupling, somatosensory EFPs and the associated CBF response provoked by whisker stimulation were evaluated in the somatosensory barrel cortex (**Fig. 9**). The amplitude of EFPs was considerably attenuated under ischemia with respect to the intact condition (107.7 ± 19.5 vs. 418.9 ± 53.5 µV, 2VO vs. intact after vehicle treatment). The application of nimodipine dramatically decreased the amplitude of evoked potentials, in the intact cortex (128.0 ± 58.6 vs. 418.9 ± 53.5 µV, nimodipine vs. vehicle in the intact group) (**Fig. 9A** and **B**).

The relative amplitude of the hyperemic response was notably smaller under ischemia than in the intact brain (6.2 ± 2.9 vs. 12.9 ± 5.4 %, 2VO vs. intact, after vehicle treatment). Treatment with nimodipine recovered the relative amplitude of the CBF response to the intact level (15.4 ± 6.7 vs. 6.2 ± 2.9 % vs. 12.9 ± 5.4 %, 2VO nimodipine vs. 2VO vehicle vs. intact vehicle). Additive to the elevation of baseline CBF achieved by nimodipine, the further improvement of the CBF response to whisker stimulation in the ischemic cortex was highly remarkable (**Fig. 9C** and **D**).
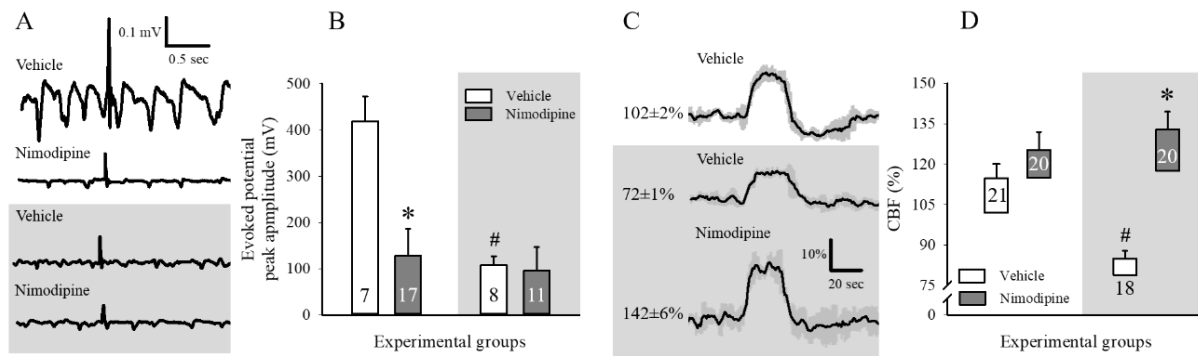
Figure 9. The impact of ischemia or pharmacological treatments on evoked field potentials (EFPs) and the coupled cerebral blood flow (CBF) response during whisker stimulation in *Experimental Project I*. Traces and bars in front of white background were taken from intact animals, while the traces and bars in front of dark gray background represent ischemia achieved with bilateral common carotid artery occlusion (2VO). **A)** Representative local field potential (LFP) traces display somatosensory EFPs during whisker stimulation. **B)** The peak amplitude of EFPs. **C)** Traces (each is the mean of 4 stimulations in an animal representative of each condition) show the CBF response to whisker stimulation. Each trace is the average of a number of individual events and are presented as mean±stdev. **D)** The relative amplitude of the CBF response to whisker stimulation. The base of each bar in the chart is set to the CBF level directly preceding whisker stimulation. Note that, nimodipine significantly decreased the amplitude of EFP in the intact cortex and recovered the amplitude of CBF response to intact level under the ischemic condition. In panel B and D, data are given as mean±stdev; sample size (i.e., the number of events analyzed) is indicated in each bar. Statistical analysis relied on a two-way ANOVA paradigm (factors: 2VO and treatment). The level of significance was defined as $p<0.05$*. A Games-Howell post hoc test was applied for group comparisons ($p<0.05$*vs. vehicle; $p<0.05$# vs. respective intact).

4.4. The impact of nimodipine on spreading depolarization

SD events were experimentally triggered in the intact brain (*Experimental Project I*) or under global forebrain ischemia (*Experimental Project I, II*) to evaluate the potential impact of nimodipine on the kinetics of SD, the associated CBF response and tissue pH variation (**Fig. 10-13**).

4.4.1. The DC potential signature of spreading depolarization

SD occurrence was confirmed by the transient negative shift of the DC potential (**Fig 10A**). In *Experimental Project I*, nimodipine in solution significantly decreased SD amplitude (-13.2±2.5 vs. -15.1±2.1 mV, nimodipine vs. vehicle in the intact condition) (**Fig. 10B**). In addition, nimodipine shortened SD duration in the ischemic cortex to the intact level (31.1±7.4 vs. 61.4±41.9 vs. 31.5±9.5 s, 2VO nimodipine vs. 2VO vehicle vs. intact vehicle) (**Fig. 10C**).
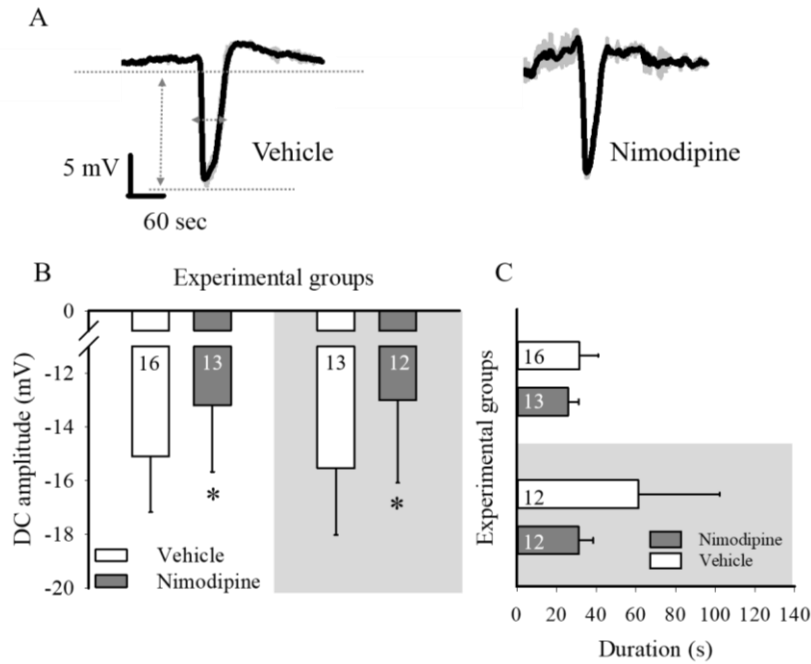
Figure 10. The impact of ischemia or nimodipine treatment on recurrent spreading depolarizations (rSDs) **A)** Traces (each is the mean of rSDs in an animal representative of each condition) demonstrate the negative DC potential shift indicative of rSDs, triggered after the ischemia onset in *Experimental Project I*. Each trace is the average of a number of individual events and are presented as mean±stdev. **B)** Amplitude of the negative DC potential shift with rSDs. **C)** Duration of the negative DC potential shift with rSDs, measured at half amplitude. In B and C, bars in front of white background represent the intact condition, while the bars in front of dark gray background stand for bilateral common carotid artery occlusion (2VO). Data are given as mean±stdev; sample size (i.e., the number of events analyzed) is indicated in each bar. Statistical analysis relied on a two-way ANOVA paradigm (factors: 2VO and treatment). The level of significance was defined as $p<0.05$* vs. vehicle. Tukey's HSD (B) or a Games-Howell (C) post hoc test was applied for group comparisons.

As expected, in *Experimental Project II*, the analysis of the DC potential signature of SDs demonstrated that nimodipine applied in the nanoparticle suspension shortened the duration of rSDs significantly with respect to control (48.07±23.29 vs. 76.25±17.2 s, nimodipine vs. vehicle) (**Fig. 11C**). Moreover, it facilitated the rate of repolarization of rSD events in particular (0.8±0.523 vs. 0.279±0.153 mV/s, nimodipine vs. vehicle) (**Fig. 11B**).
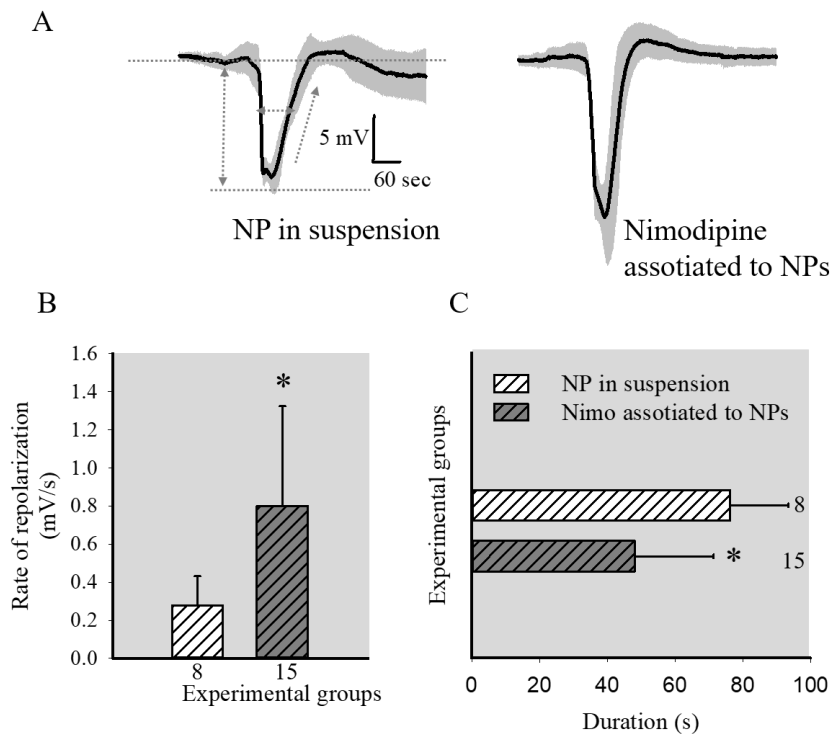
Figure 11. The impact of ischemia or nimodipine treatment on recurrent spreading depolarizations (rSDs). **A)** Traces demonstrate the negative DC potential shift indicative of rSDs in *Experimental Project II*. Each trace is the average of a number of individual events and are presented as mean±stdev. **B)** Rate of repolarization of the negative DC potential shift with rSDs. **C)** Duration of the negative DC potential shift with rSDs, measured at half amplitude. Data are given as mean±stdev; sample size (i.e., the number of events analyzed) is indicated in each bar. Statistical analysis relied on a one-way ANOVA paradigm. The level of significance was defined as $p < 0.05$* vs. vehicle.

4.4.2. The local cerebral blood flow response to spreading depolarization

The share of the individual elements in the CBF response to SD is variable across animal species and anesthesia protocols and appears to change remarkably according to the actual metabolic status of the tissue [27]. Considering the different anesthesia protocols during the period of actual data acquisition (i.e., α-chloralose in *Experimental Project I*, and isoflurane in *Experimental Project II*), we found different kinetics of the CBF responses in *Experimental Project I* and *II*. The initial hypoperfusion proved to be detectable only occasionally, therefore the analysis focused on the peak hyperemic element of the CBF response.

In *Experimental Project I*, the CBF response to SD consisted of 4 elements, starting with a transient hypoperfusion, followed by a peak and then a late hyperemia, and concluded by a long-lasting oligemia [27]. The kinetics of the observed CBF responses exhibited a spectrum considering the weight of late hyperemia in the signature. Further, the presence of the late hyperemic element served as the basis for CBF response classification to distinguish CBF

response Type 1 characterized by peak hyperemia only, from CBF response Type 2 that included late hyperemia in addition to the peak hyperemia **(Fig 12A)**. A semi-quantitative approach of ours indicated that the likelihood for Type 1 and Type 2 CBF responses to evolve was near equal in the vehicle-treated, intact condition. Conversely, ischemia, or treatment with nimodipine, allowed late hyperemia to emerge at a clearly higher incidence **(Fig 12B)**. The amplitude of peak hyperemia was conserved over experimental groups, except for nimodipine treatment in the ischemic condition, which augmented peak hyperemia amplitude (relative change: 185 ± 62 vs. 131 ± 66 %, nimodipine vs. vehicle in the 2VO group) **(Fig 12C)**. The duration of hyperemia (i.e., peak, and late hyperemia together) was not significantly altered by ischemia or the treatment.
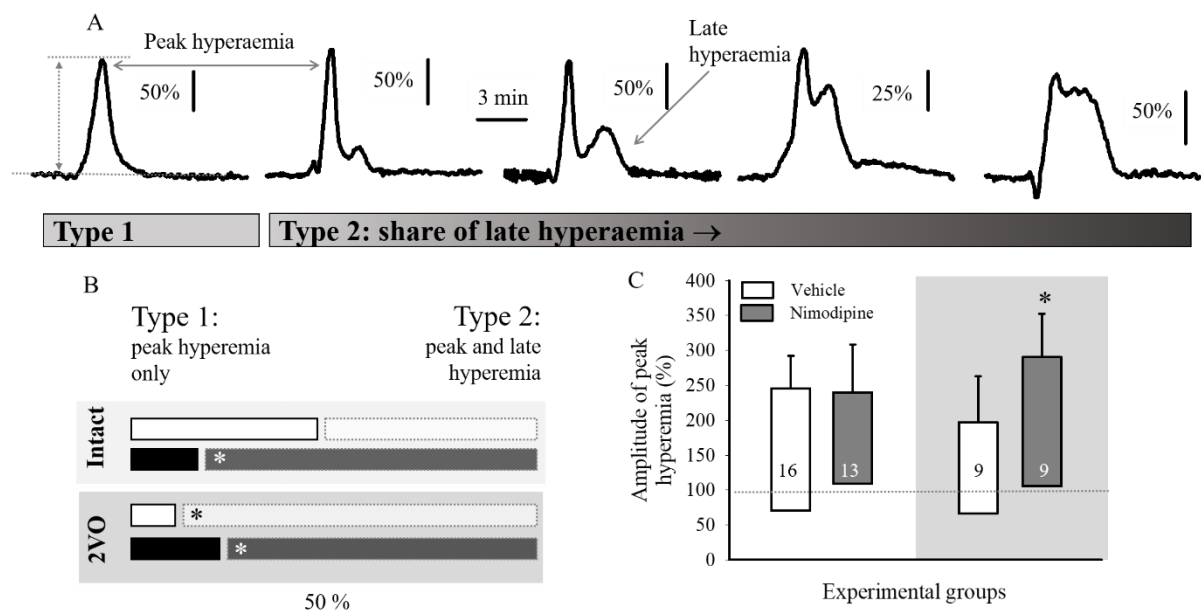
Figure 12. The impact of ischemia or pharmacological treatments on the cerebral blood flow (CBF) response to recurrent spreading depolarization (rSD) events in *Experimental Project I*. **A)** Representative traces demonstrate the spectrum of the kinetics of the CBF response considering the weight of late hyperemia in the signature. The CBF response was classified as Type 1 whenever peak hyperemia was obvious, with late hyperemia being undetectable. The CBF response was labelled Type 2, when both peak and late hyperemia could be identified. **B)** Occurrence of Type 1 and Type 2 CBF responses is depicted with respect to all of the CBF responses analyzed being taken as 100% in each experimental group. Horizontal bars with black outline (left) depict the share of Type 1, while bars with grey outline (right) represent the ratio of Type 2 CBF responses. Note that the two types were represented equally (i.e., near 50%) in the vehicle-treated, intact groups. Pearson chi-square test for association indicated a significant effect (value: 16.996, P < 0.017). Calculating column proportion by z test with Bonferroni correction identified a significant shift in Type 1 and Type 2 ratios for groups labelled (*). **C)** Amplitude of peak hyperemia. The base of each bar in the chart is set to the CBF level preceding rSD events. Bars in front of white background represent the intact condition, while the bars in front of dark gray background stand for bilateral common carotid artery occlusion (2VO). Data are given as mean ± stdev; sample size (i.e., the number of events analyzed) is indicated in each bar. Statistical analysis relied on a two-way ANOVA paradigm (factors: ischemia, and treatment). The level of significance was defined as *p<0.05. Tukey's HSD test was applied for group comparisons.

In contrast with the CBF response to SD under α-chloralose anesthesia, SD related CBF response in isoflurane anesthetized rats in *Experimental Protocol II*, included an initial transient hypoperfusion, followed by a peak hyperemia and a long lasting oligemia [40], but we did not detect the late hyperemic element. As expected, nimodipine delivered by nanoparticles significantly enhanced the amplitude (48.15±42.04 vs. 17.29±11.03 %, nimodipine vs. vehicle) (**Fig. 13B**) and the magnitude of peak hyperemia in response to rSDs (4604.43±2572.3 vs. 2368.05±1324.71 %*s, nimodipine vs. vehicle) (**Fig. 13C**).
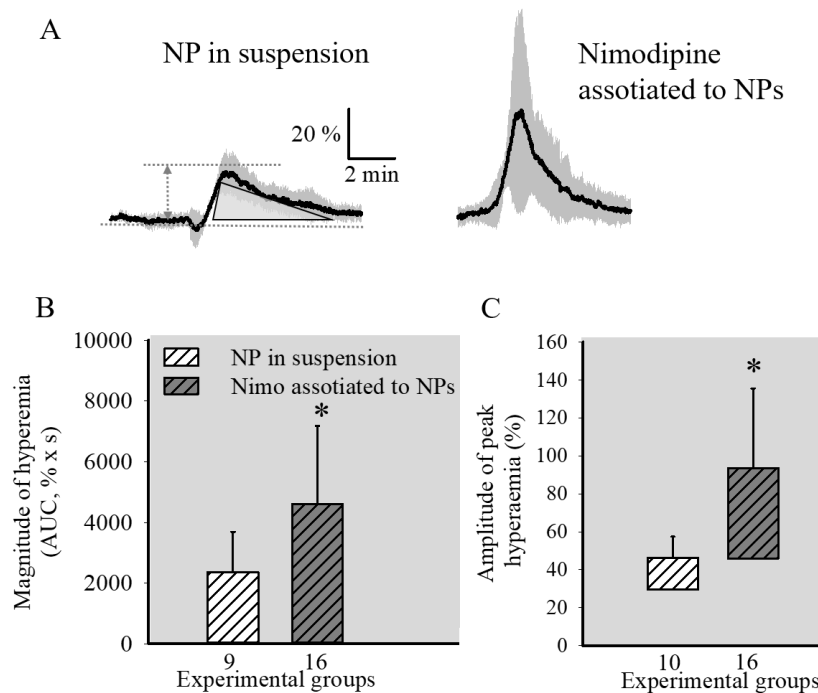
Figure 13. The impact of ischemia or pharmacological treatments on the cerebral blood flow (CBF) response to recurrent spreading depolarization (rSD) events in *Experimental Project II*. **A)** Traces demonstrate the kinetics of CBF response to rSD events. Each trace is the average of a number of individual events and are presented as mean±stdev. **B)** Magnitude (i. e. area under the curve, AUC) of peak hyperemia. **C)** Amplitude of peak hyperemia. The base of each bar in the chart is set to the CBF level preceding rSD events. Data are given as mean±stdev; sample size (i.e., the number of events analyzed) is indicated below each bar. Statistical analysis relied on one-way ANOVA paradigm. The level of significance was defined as $p<0.05*$ vs. vehicle.

4.4.3.　　　Tissue pH variations related to spreading depolarization

In *Experimental Project II*, we measured extracellular tissue pH variations corresponding to ischemia induction and SD events. As presented above, ischemia induction causes an acidic tissue pH shift from the neutral 7.3-7.4 to 7.06±0.30. Tissue pH variations associated with SD events started with a rapid, short alkaline shift followed by a longer-lasting, dominant, transient acidosis [40] (**Fig. 14**). Tissue pH did not fully recover and remained typically mildly acidic after SD1 (pH 7.14±0.29 vs. 7.23±0.28, prior to rSDs vs. prior to SD1). Nimodipine treatment had no measurable impact on the initial alkaline shift but modified the kinetics of the subsequent transient acidosis. As such, nimodipine delivered by nanoparticles facilitated the rate of return from the acidic shift with rSDs (0.01±0.006 vs. 0.005±0.002 pH unit/s, nimodipine vs. vehicle) (**Fig. 14C**) and shortened the duration of acidosis with rSDs (65.46±20.2 vs. 138.3±66.07 s, nimodipine vs. vehicle) (**Fig. 14B**). Consequently, the magnitude of acidosis expressed as AUC was substantially reduced in the nimodipine compared to vehicle group (25.75±10.69 vs. 49.46±23.38 pH unit*s, nimodipine vs. vehicle) (**Fig. 14D**).
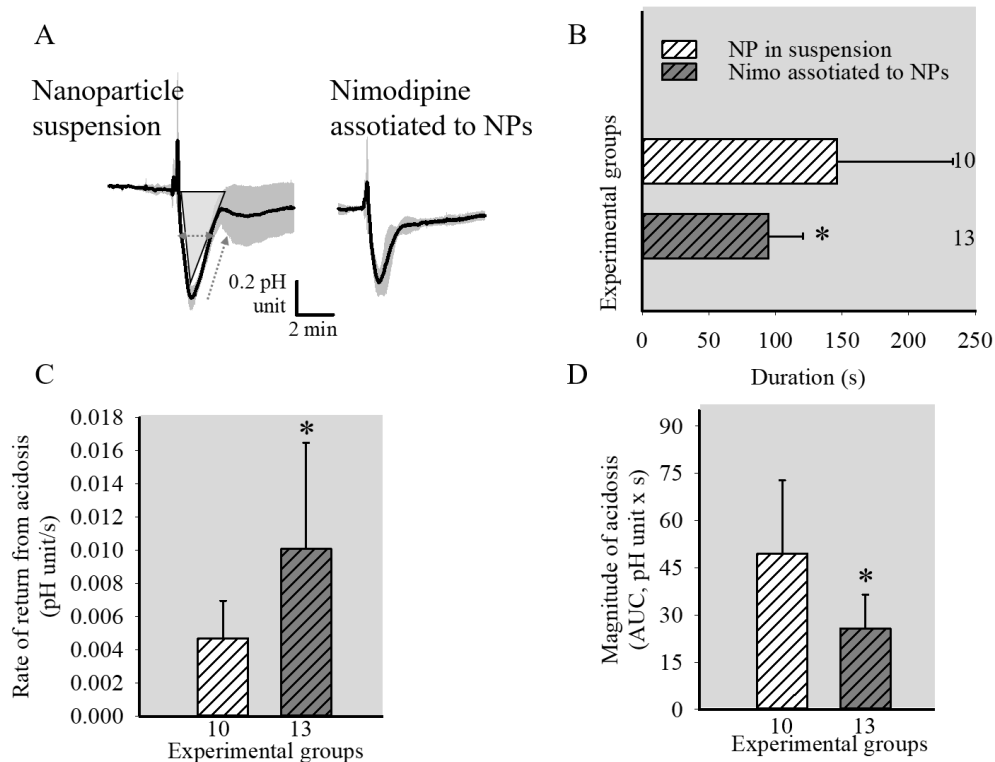
Figure 14. The impact of nimodipine delivered with nanoparticles on the tissue pH response related to recurrent spreading depolarization events (rSDs) in *Experimental Project II*. **A)** Traces demonstrate the kinetics of pH response to rSD events. Each trace is the average of a number of individual events taken from separate animals and are presented as mean±stdev. **B)** Duration of tissue acidosis taken at half amplitude. **C)** Rate of return from tissue acidosis. **D)** Magnitude (i. e. area under the curve, AUC) of tissue acidosis. Note that, nimodipine facilitated the rate of return from acidosis, moreover it shortened the duration and reduced the magnitude of the acidotic shift with SD. Data are given as mean±stdev, sample size (i.e., the number of events analyzed) is indicated near each bar. Statistical analysis relied on one-way ANOVA paradigm. The level of significance was defined as $p < 0.05$* vs. vehicle.

4.5. Histology

In order to explore whether the chitosan nanoparticles used here might trigger neuroinflammatory reactions (a potential unfavorable side effect of the drug delivery approach), we estimated microglial activation in immune-stained brain sections, at the end of *Experimental Project II*. Microglia immunolabeled for Iba1 appeared to be activated in the cerebral cortex ipsilateral to the initiation of SD events, as shown by their sparser processes and rounded, amoeboid shape (**Fig. 15A**). Microglia activation was quantitatively expressed by a ramification index [78] representing the density of microglial processes. The ramification index was remarkably reduced in the ipsilateral compared to the contralateral somatosensory cortex (e.g., 398±203 vs. 1118±300, ipsi- vs. contralateral in the vehicle group) (**Fig. 15A**). The hemisphere-specific reduction of the ramification index was attributed to SD, because it was observed in rats with bilateral craniotomy (unilateral SD induction), as well (201±102 vs.

483±244, ipsi- vs. contralateral). The application of the nanoparticle suspension alone (vehicle) or incorporating nimodipine did not reduce the ramification index any further compared to aCSF-rinsed preparations (control) (443±208 vs. 398±203 vs. 284±107, nimodipine vs. vehicle vs. control; ipsilateral) (**Fig. 15A**). Thus, the administration of nanoparticles on the cortical surface did not produce a detectable potentiation of microglia activation.

We labeled viable neurons with NeuN immunohistochemistry to estimate (i) the degree of early neurodegeneration SD might cause in the acute phase of global forebrain ischemia, and (ii) the potential neuroprotection achieved by nimodipine (**Fig. 15B**). We screened the somatosensory cortex (i.e., over the striatum) distant to the site of SD elicitation (i.e., over the hippocampus), with the aim to exclude areas from the analysis, in which neurodegeneration might have been caused by topical KCl application to trigger SD. In some animals, the reduced relative area covered by NeuN-immunolabeled neurons indicated early neurodegeneration in the cerebral cortex ipsilateral to the initiation of SD events (**Fig. 15B**), albeit the quantitative analysis did not reveal significant SD-related neuron loss (26.9±5.0 vs. 29.1±4.7 %, ipsi- vs. contralateral in the vehicle group) (**Fig. 15B**). NeuN labeling was not enhanced in the nimodipine-treated group in a statistically meaningful manner (29.0±4.8 vs. 26.9±5.0 %, nimodipine vs. vehicle in the ipsilateral cortex) (**Fig. 15B**).
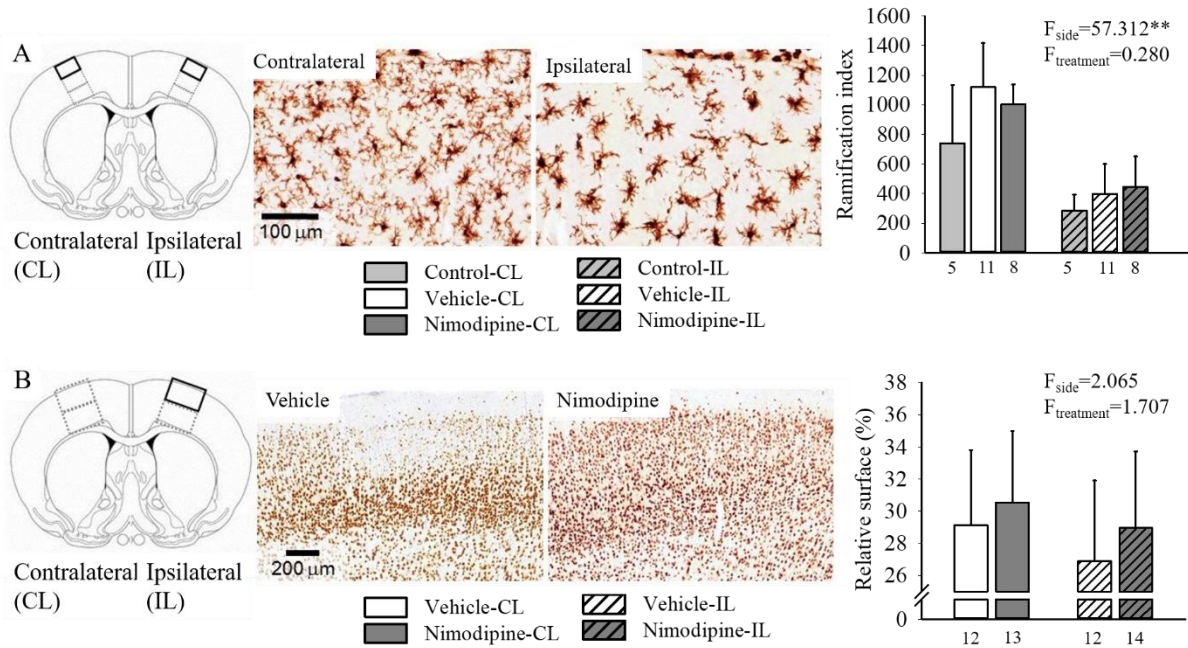
Figure 15. The impact of the topical application of the nanoparticle suspension with or without nimodipine on microglia activation and neuronal viability in *Experimental Project II*. **A)** Microglia immunolabeled for Iba1 appeared to be activated in the cerebral cortex ipsilateral to the initiation of spreading depolarization (SD) and craniotomy. The application of the nanoparticle suspension alone (vehicle) or incorporating nimodipine did not trigger additional microglia activation compared to aCSF-rinsed preparations (control). Microglia activation was expressed by a ramification index representing the density of microglial processes. **B)** The relative area covered by NeuN-immunolabeled neurons expressed early signs of neurodegeneration in the cerebral cortex ipsilateral to the initiation of SD and craniotomy. Nimodipine did not prevent neurodegeneration in a statistically meaningful manner. Data are given as mean±stdev, sample size (i.e., the number of events analyzed) is indicated below each bar. Statistical analysis relied on a two-way ANOVA paradigm. The level of significance was defined as $p<0.05^*$.

5. Discussion

Here we set out to explore whether nanoparticles designed to release nimodipine in response to pH decreasing below the physiological range (pH 7.3-7.4) are effective to counteract some injury markers in experimental cerebral ischemia. The model used reproduces conditions typical of the ischemic penumbra [3, 40], which is indicated by tissue perfusion ranging between 20 and 40 % of baseline, and tissue pH dropping to 6.9–7.1 after ischemia induction (**Fig 3**). We hypothesized, that nanoparticles are suitable for targeting drug release to the ischemic region in the nervous tissue. Tissue acidosis caused by ischemia or SD occurrence was supposed to trigger effective drug release in the injured region. We have selected nimodipine, an L-type VGCC antagonist as the drug to be delivered, because its cerebral vasodilator, SD limiting and neuroprotective actions have been widely acknowledged [67, 80-83] to be used as a reference for the nanoparticle study. We presumed that nimodipine administered with nanoparticles should exert its expected vasodilator and neuroprotective effects and should impede SDs propagating over the penumbra.

5.1. Acidosis linked to cerebral ischemia can be employed as a trigger for targeted drug delivery

In *Experimental Project II*, nimodipine associated to pH-responsive nanoparticles did not achieve CBF elevation prior to ischemia induction, when tissue pH was physiological, which confirms that nimodipine was not dissociated from the nanoparticles at near neutral tissue pH. Subsequent to the induction of ischemia and the related transient tissue acidosis, baseline CBF was found to be higher in the nimodipine-treated compared to the vehicle group, which is consistent with the known cerebrovascular action of nimodipine [84], and we interpreted it as the *in vivo* verification of pH-sensitive drug release [74] (**Fig 8**).

5.1.1. Recent advantages in nanomedicine

Although disorders of the brain (i.e., cerebrovascular disorders, neurodegenerative diseases, or tumors) are one of the leading causes of death and long-term disability worldwide, the barriers of the central nervous system (BBB and blood-cerebrospinal fluid barrier) represent important pharmacological challenges of systemic drug-treatment. Nanotechnology can be applied in a wide range of diseases for diagnostic and therapeutic drug delivery of brain disorders. Compounds fabricated by this advanced technology can promote drug transport through a variety of biological membranes and/ or prolong their circulation time in the blood [71, 85].

Nanoparticles fall under a structurally heterogenic group of nano-sized drug delivery systems (DDSs), with different preparation, composition, shape, size, hydrophilicity, penetration properties, conductivity, or surface charge [86]. Due to their special properties, nano-sized DDSs could become potential therapeutic methods. Their surface to volume ratio is relatively high, that is why reactions (i.e., drug release, penetration, binding to specific receptors) between particles and their environment take place on a relatively large surface. They can interact with biological systems at a molecular and supra-molecular level, so their biological responses can be designed to minimize their side effects [87]. Nano-sized DDSs can modify and ameliorate the biodistribution, bioavailability and pharmacokinetics of agents. Moreover, they can carry various types of molecules (i.e., nucleotides, peptides, proteins or low-molecular weight compounds), or more agents simultaneously for combination therapy. The design of the nano-sized DDSs can protect the drugs from disadvantageous metabolism. We can target their release to specific cell types or via small changes of an environmental factor (i.e., pH, temperature, magnetic field, light, ultrasound) [71].

5.1.2.   Tissue acidosis to guide neuroprotective intervention in ischemic stroke

Over the last few years, an increasing number of studies addressed the application of nanotechnology for the treatment of ischemic stroke. Nano-sized DDSs to cross the BBB should be smaller than 100 nm, biodegradable, biocompatible, non-toxic, and stable in blood. They should be able to penetrate the BBB, to carry different types of agents, and should not trigger neuroimmune reactions. In the best scenario, nano-sized DDSs have prolonged circulation time and controlled drug release [88]. The application of biocompatible and biodegradable, natural, or synthetic macromolecular polymeric nanocarriers offers substantial promise in therapeutics [89-91]. Among others, stimulus responsive nanoparticles present the opportunity to initiate drug release by local (patho)physiological biochemical stimuli (e.g., homeostatic, redox, enzymatic, tissue pH) [92-94], which are intrinsic and restricted to the diseased tissue, and are closely related to the progression of the disease condition. These bioresponsive nanomaterials are also known as "smart" nanosystems [95]. A negative pH shift from the neutral 7.3-7.4 to below 7.0 units, for instance, can initiate conformational or solubility changes in various smart nanosystems, including polysaccharide chitosan nanoparticles, to allow drug release [73, 74, 95]. In accordance, the acidic local tumor environment created by intensive or dysregulated glucose metabolism [96-98] has been utilized as a specific trigger for drug release in the treatment of solid cancers [73, 99, 100].

41

The achievements of cancer nanomedicine have inspired the application of nanotechnology in the therapy of ischemic stroke, especially because these diverse disease entities share some distinct pathophysiological processes [101]. Along with the disintegration of microvascular ultrastructure, intensified generation or failing clearance of ROS, and cellular immune reactions [101], tissue acidosis occurs in tumors [96-98], as well as in ischemic brain tissue.

5.1.3. Neuroimmune responses against nanoparticles

In *Experimental Project II*, we intended to examine whether chitosan nanoparticles may induce a neuroimmune response at the brain tissue in contact with the nanoparticles. Chitosan, a derivative of chitin, is a biocompatible, biodegradable, natural polysaccharide, which has been considered as immune adjuvant in cancer therapy [102, 103]. Microglia form the active immune defense of the brain, and their reaction to inflammatory stimuli is accompanied by their typical morphological alteration (i.e., retraction of processes, amoeboid form). We, therefore, labeled microglia to estimate their potential activation by chitosan nanoparticles in our experimental model. The application of chitosan nanoparticle suspension to the exposed cortical surface did not enhance microglia activation with respect to aCSF rinsed preparations in our experiments, which suggests that chitosan nanoparticles themselves did not trigger a detectable local immune reaction in the cerebral cortex **(Fig 15)**.

Administration of nano-sized particles to the body, irrespectively of the route of administration (i.e., topical, enteral, parenteral routes), inevitably initiates an interaction with the immune system, so understanding the potential risk of application of new nanomaterials is a fundamental question. Nanoparticles can interact with cellular and subcellular (i.e., receptors, proteins) parts of the immune system, activating signaling cascades, causing unpredictable, harmful immune responses (i.e., allergy, autoimmune diseases, cancer). The interaction of nanoparticles with the immune system is determined by their physicochemical properties (i.e., size, shape, surface, hydrophobicity). The bigger the nanoparticle, the smaller its surface to volume ratio, which influences the immune response. Although, there is no linear correlation between nanoparticle size and immune response, several studies described that, smaller nanoparticles (up to 200 nm) are drained to the lymph nodes (resident dendritic cells), while larger ones (500-1000 nm) accumulate in the macrophages of the liver (Kupffer cells). It was demonstrated, that increasing level of hydrophobicity of nanoparticles leads to better cellular internalization and costimulatory marker-expression in immune cells [104].

5.2. The effect of nimodipine on the regulation of local cerebral blood, neuronal function, and local tissue pH

Nimodipine, a dihydropyridine derivative, inhibits Ca^{2+} influx to VSMCs and causes vasodilation. In addition, nimodipine blocks neuronal L-type VGCCs, as well, mitigates neuronal Ca^{2+} overload, and achieves neuroprotection under ischemic stress [82]. In the incomplete global forebrain ischemia model used, we first assessed drug effect on physiological neuronal activation (i.e., achieved by somatosensory stimulation) and the coupled functional hyperemic response. Next, we focused on the impact of the pharmacological treatments on SD and the associated CBF and pH response. SD is an ischemic preconditioning stimulus when triggered in intact tissue [105] and represents a pathophysiological process as it occurs due to extracellular K^+ and glutamate accumulation in ischemic brain [20, 26].

Before the detailed discussion of drug effects, it must be appreciated that hyperemia in response to SD was markedly accentuated under α-chloralose anesthesia (used in *Experimental Project I*) (relative amplitude: 191 ± 61 and 151 ± 96 %, intact and under ischemia, respectively), with respect to that seen under isoflurane anesthesia (used in *Experimental Project II*) in our previous work (e.g., 51 ± 38 and 21 ± 11 %, intact and under ischemia, respectively, Varga et al., 2016; 76 ± 12 and 21 ± 9 %, intact and under ischemia, respectively, Menyhárt et al., 2017). Moreover, late hyperemia in the CBF response to SD was revealed very often under α-chloralose anesthesia as seen in *Experimental Project I*, while it was seldom encountered in many of our previous studies using isoflurane [40, 106, 107], and in *Experimental Project II*. Finally, the global ischemia model we routinely use produces a considerable drop of CBF following 2VO under isoflurane anesthesia (e.g., to $27 \pm 13\%$, Varga et al., 2016, to $41 \pm 9\%$; Menyhárt et al., 2015) – this drop proved to be considerably more moderate under α-chloralose anesthesia in *Experimental Project I* (**Fig 8**) [106, 107].

5.2.1. Nimodipine effectively improves neurovascular coupling, subsequently augments functional hyperemia

In *Experimental Project I*, the impact of nimodipine on the regulation of local CBF was investigated by somatosensory stimulation. In our experiments, whisker stimulation was applied to investigate functional hyperemia in the barrel cortex of anaesthetized rats. In the barrel cortex of rats somatotopy is noticeable, stimulation of a distinct whisker evokes neuronal activation, and subsequent CBF elevation, in the adherent cortical region [108].

Since the brain has limited capacity to store energy, it needs continuous energy supply, which is maintained by continuous perfusion through its complex web of blood vessels. Several

mechanisms guarantee the continuous nutrient and O_2 transport to the brain. One of them is neurovascular coupling, which is a coordinated interaction among activated neurons, astrocytes, and contractile cells of the vessel wall. At different levels of the vascular tree, different cell types regulate local CBF. At the level of penetrating arteries and parenchymal arterioles, neurons, astrocytes and VSMCs compose the unit of local CBF regulation, called neurovascular unit. At the capillary level, the contractile cells are pericytes, that share a common basement membrane with endothelial cells. VSMCs and pericytes are covered by the endfeet of astrocytes, and all these three cell types are innervated by neurons at each level of the vascular tree. Because of their proper anatomical position, astrocytes transfer the information from activated neurons directly to contractile cells, regulating the cerebral microcirculation [109].

It is a novel finding of the presented work, that, in addition to baseline CBF elevation, nimodipine profoundly augmented functional hyperemia in response to somatosensory stimulation, without enhancing EFP amplitude under ischemia. Nimodipine remarkably decreased EFP amplitude in the intact cortex, while the relative magnitude of the flow response was maintained **(Fig 9)**. Both observations imply that the enhancement of functional hyperemia by nimodipine is disproportionate with respect to EFP amplitude. This suggests that nimodipine augmented the amplitude of the CBF response (irrespective of the intensity of neuronal activation initiated by somatosensory stimulation), possibly by potentiating the release of vasodilator substances or the efficacy of vasodilator signaling cascades. Since vasodilator prostaglandins and epoxyeicosatrienoic acids are produced by astrocytes during neurovascular coupling [110], and L-type VGCCs are present in the astrocyte plasma membrane [111], astrocytes may be involved in the nimodipine-related enlargement of functional hyperemia, without neuronal contribution being proportionally increased in the first place.

5.2.2.   Nimodipine inhibited spreading depolarization evolution and augmented hyperemia in response to SD events

Nimodipine application reduced SD size (amplitude, and duration at half amplitude), in agreement with previous reports applying nimodipine at the concentration used in our studies [62, 63] **(Fig 10, 11)**. Neurons express L-type VGCCs, which have been implicated in the modification of neuronal excitability and are a well-known target of nimodipine [82]. Although pharmacologically decreased SD amplitude is often interpreted as a sign of protection [112], the lack of a clear-cut association between SD amplitude and histological or neurological damage imposed creates persistent controversies. Our data support earlier observations that the number of rSDs, the cumulative duration of SDs, and the inability of the tissue to recover from

SD (i.e., long SD duration) correlate with injury progression [20]. Nimodipine shortened SD duration, which may be accepted as a sign of its protective potential. SD is associated with neuronal Ca^{2+} loading, in part via ionotropic glutamate receptors, such as the NMDAR [26]. The reduction of the SD-associated Ca^{2+} accumulation has thus emerged as a promising target to achieve SD inhibition. For example, low dose ketamine (an NMDAR blocker) applied to brain slices was shown to reduce Ca^{2+} load and to facilitate the recovery from SD [113]. In our study, nimodipine is thought to have inhibited Ca^{2+} influx to neurons via L-type VGCCs, which also caused the more rapid recovery from SD. These results suggest that the attenuation of neuronal Ca^{2+} load (either via NMDAR blockade or L-type VGCC inhibition) shortens SD duration. To further evaluate the neuroprotective potential of the treatment, we labeled viable neurons with NeuN immunocytochemistry and quantified neuronal density in the cerebral cortex. Even at this early time point after ischemia induction, we observed in some animals less dense NeuN staining in the parietal cortex where SDs propagated, compared to the contralateral hemisphere exposed to ischemia alone, but nimodipine did not rescue neurons to a statistically meaningful degree at this endpoint **(Fig 15)**.

5.2.3. Nimodipine potently reduced the degree of SD-related acidosis

The use of pH-sensitive microelectrodes in our preparation offered the unique opportunity to assess the impact of nimodipine on the SD associated transient tissue acidosis **(Fig 14)**, an action of nimodipine not screened before. The SD-related acidosis, which has been linked to the accumulation of lactate [45, 46] was previously contemplated to exacerbate ischemic injury and jeopardize the survival of penumbra tissue [40], therefore its inhibition is expected to be beneficial. Here we have observed that nimodipine potently reduced the degree of SD-related acidosis. Similarly, intravenously administered nimodipine was shown to moderate tissue acidosis in experimental focal cerebral ischemia [114, 115], which was attributed to the direct facilitation of metabolic lactate clearance, independent of perfusion rate [115, 116]. It is thus conceivable that the inhibition of Ca^{2+} entry to neurons by nimodipine [82] may support mitochondrial function and oxidative lactate degradation [116], which may reduce the acid load associated with SD, as seen here. It is also reasonable to argue that the shorter duration of SD related acidosis due to nimodipine is consistent with the shorter duration of SD itself, and the primary effect of nimodipine was the inhibition of SD, causing a secondary reduction of the associated tissue acidosis.

6. Main observations and conclusion

The aim of our study was to explore whether nimodipine loaded pH-sensitive nanoparticles can be used effectively to reduce detrimental outcomes in experimental global cerebral ischemia.

- The work demonstrates that tissue **acidosis linked to cerebral ischemia can be employed as a trigger for targeted drug delivery**. Nimodipine associated to pH-responsive nanoparticles did not achieve CBF elevation prior to ischemia induction, when tissue pH was physiological, which confirms that nimodipine was not dissociated from the nanoparticles at physiological tissue pH (pH 7.3-7.4). After the induction of ischemia and the related transient tissue acidosis, baseline CBF was found to be higher in the nimodipine-treated compared to the vehicle group, which is interpreted as the *in vivo* verification of pH-sensitive drug release [74].

- Moreover, immunohistochemical examinations showed that the applied **chitosan nanoparticles did not activate microglia** in the brain.

Additionally, we investigated the impact of topically administered nimodipine in the intact and ischemic rat brain.

- By the topical application of nimodipine, we found that nimodipine **inhibited SD evolution**, possibly by blocking Ca^{2+} entry to nerve cells, and **augmented hyperemia in response to SD** events in the ischemic rat brain. Moreover, it potently **reduced the degree of SD-related acidosis**.

- The data generated here support the concept that L-type VGCC inhibition by **nimodipine** effectively **improves neurovascular coupling**, particularly under cerebral ischemia, **augments functional hyperemia** in response to somatosensory stimulation especially under ischemia, in addition to achieving a general, constitutive vasodilator effect.

- In addition, nimodipine-mediated vasodilation and neuroprotection can be achieved by pH-responsive chitosan nanoparticles applied directly to the brain surface.

7. Future perspectives

These results are encouraging, and also raise a number of further considerations for the potential biomedical application of the principle of acidosis guided drug targeting. We washed the nanoparticle suspension directly to the exposed cortical surface in our pre-clinical model, which offers data relevant for potential intracerebroventricular, intraparenchymal or intrathecal drug delivery [117]. Yet, all these methods are significantly invasive. Therefore, other routes of administration that are more realistic in routine clinical care need to be tested. An obvious option appears to be intravenous infusion. For this approach, the BBB permeation of the chitosan nanospheres must be evaluated, because particles larger than 12-30 nm may not cross the BBB [118]. Further, the retention of nanoparticles in non-target tissues (e.g., cells of the reticuloendothelial system) could decrease the number of circulating nanoparticles before their penetration to the brain [119]. Finally, potentially low tissue pH prevailing in peripheral organs or body fluids (e.g., in the respiratory system or the gastrointestinal tract) would perceivably cause off-target drug release. Although the size of the nimodipine-loaded nanoparticles in our study was small enough for BBB penetration (i.e., 4-6 nm) [74], the BBB permeability of chitosan nanoparticles may be improved by functionalizing chitosan with antibodies that recognize receptors specific to BBB endothelial cells (e.g., transferrin receptors) [120, 121]. This should initiate the receptor-mediated transcytosis of the nanospheres. In addition, cerebral ischemia may derange the BBB and enhance non-selective transendothelial vesicular transport or loosen the tight junctions between adjacent endothelial cells [122]. This may allow drug carriers to reach the nervous tissue along with the extravasation of blood plasma. Of note, SD itself can increase endothelial transcytosis and paracellular diffusion at the BBB [123, 124], and was found to facilitate drug delivery to the brain tissue [123]. Finally, the intracarotid, rather than intravenous route of infusion of drug-loaded nanocarriers should provide direct access to the brain [125], which could substantially reduce off-target retention and drug release at the periphery.

The intranasal application of the nanoparticles may be an alternative route of drug administration. Chitosan, in fact, displays very good adhesion to the nasal mucosa due to the positively charged nanoparticle surfaces [126], and enhances absorption through the nasal mucosa by disrupting the intercellular tight junctions of the epithelium [127, 128]. However, the nasal mucosa is acidic (pH 5.5-6.5). This condition contraindicates the nasal administration of acid responsive nanoparticles targeting the brain, unless the nanoparticles are supplied with a protective coating during their passage through the nasal mucosa, which the particles should shed before reaching the brain.

8. Summary

Background: Ischemic stroke is a leading cause of death and disability worldwide. Yet, the effective therapy of focal cerebral ischemia has been an unresolved challenge. We propose here that ischemic tissue acidosis, a sensitive metabolic indicator of injury progression in cerebral ischemia, can be harnessed for the targeted delivery of neuroprotective agents. Ischemic tissue acidosis, which represents the accumulation of lactic acid in malperfused brain tissue is significantly exacerbated by the recurrence of SD events. Deepening acidosis itself activates specific ion channels to cause neurotoxic cellular Ca^{2+} accumulation and cytotoxic edema. These processes are thought to contribute to the loss of the ischemic penumbra. Importantly, acidosis in the ischemic penumbra may also be used to guide therapeutic intervention. Nimodipine, an L-type VGCC antagonist dilates cerebral arterioles, but its systemic administration may cause potential side effects (mainly hypotension). We have constructed chitosan nanoparticles as drug carriers, which release nimodipine in response to decreasing pH typical of cerebral ischemia. Here we have set out to evaluate this nanomedical approach to deliver nimodipine selectively to acidic ischemic brain tissue.

Methods: Two sets of experiments are presented in this thesis. In *Experimental Project I*, nimodipine was applied in solution (100 µM), then global forebrain ischemia was induced in half of the animals by bilateral common carotid artery occlusion under isoflurane anesthesia. Functional hyperemia in the somatosensory cortex was created by mechanical stimulation of the contralateral whisker pad under α-chloralose anesthesia. SD events were elicited subsequently by 1 M KCl. LFP and CBF in the parietal somatosensory cortex were monitored by electrophysiology and LDF. In *Experimental Project II*, nimodipine was associated with pH-sensitive nanoparticles in suspension. After washing the nanoparticle suspension with or without nimodipine (100 µM) on the exposed brain surface of anesthetized rats, both common carotid arteries were occluded to create forebrain ischemia. SDs were elicited by 1 M KCl to deepen the ischemic insult. LFP, CBF and tissue pH were recorded from the cerebral cortex. Microglia activation and neuronal survival were evaluated in brain sections by immunocytochemistry.

Results: Nimodipine in solution attenuated evoked potentials and SD. In addition to the elevation of baseline CBF, nimodipine augmented hyperemia in response to both somatosensory stimulation and SD, the drug effect was particularly discernable under ischemia. Ischemia-induced tissue acidosis initiated nimodipine release from nanoparticles, confirmed by the significant elevation of baseline CBF. Nimodipine shortened the duration of both SD itself,

and the associated tissue acidosis, moreover it enhanced the SD-related hyperemia. Chitosan nanoparticles did not activate microglia.

Conclusions: The administered nanoparticles release nimodipine in acidic tissue environment, which reliably delineates sites at risk of injury. The data support the concept that tissue acidosis linked to cerebral ischemia can be employed as a trigger for targeted drug delivery. Nimodipine-mediated vasodilation and SD inhibition can be achieved by pH-responsive chitosan nanoparticles applied directly to the brain surface. Ultimately, this approach may offer a new way to treat stroke patients with the hope of more effective therapy, and better stroke outcome.

Acknowledgements

I am extremely grateful to my supervisors, Dr. Eszter Farkas and Prof. Ferenc Bari for their invaluable advice, continuous support, and patience during my PhD study. Their immense knowledge and plentiful experience have encouraged me throughout of my academic research and daily life.

I am deeply grateful to Dr. Írisz Szabó and Dr. Ákos Menyhárt for their advice and technical support on my study. I would like to thank all the members in the Group of Cerebral Blood Flow and Metabolism: Rita Frank, Orsolya Ivánkovitsné Kiss, Dr. Dániel Varga, Dr. Viktória Varga, and Dr. Péter Makra.
I would like to say thanks to Dr. Ádám Institóris for introducing me to the world of science and laboratory work.

I would also like to thank Prof. Dr. Ferenc Peták for supporting my work at the Department of Medical Physics and Medical Informatics.
I would like to thank Prof. Gábor Jancsó for accepting my application to the Theoretical Medicine Doctoral School.

And last, but not least, words cannot describe how grateful I am to my family. I would like to express my gratitude to my parents, siblings, and grandparents for their unwavering support and belief in me. I thank from the bottom of my heart to my husband, Bence, and our little son, Gergő, for their unbreakable love and support. Without their tremendous understanding and encouragement in the past few years, it would have been impossible for me to complete my study.

9. References

1.   Powers, W.J., et al., *2018 Guidelines for the Early Management of Patients With Acute Ischemic Stroke: A Guideline for Healthcare Professionals From the American Heart Association/American Stroke Association.* Stroke, 2018. **49**(3): p. e46-e110.

2.   Lipton, P., *Ischemic cell death in brain neurons.* Physiol Rev, 1999. **79**(4): p. 1431-568.

3.   Astrup, J., et al., *Cortical evoked potential and extracellular K+ and H+ at critical levels of brain ischemia.* Stroke, 1977. **8**(1): p. 51-7.

4.   Astrup, J., B.K. Siesjö, and L. Symon, *Thresholds in cerebral ischemia - the ischemic penumbra.* Stroke, 1981. **12**(6): p. 723-5.

5.   Paciaroni, M., V. Caso, and G. Agnelli, *The concept of ischemic penumbra in acute stroke and therapeutic opportunities.* Eur Neurol, 2009. **61**(6): p. 321-30.

6.   Lo, E.H., *A new penumbra: transitioning from injury into repair after stroke.* Nat Med, 2008. **14**(5): p. 497-500.

7.   Leigh, R., et al., *Imaging the physiological evolution of the ischemic penumbra in acute ischemic stroke.* J Cereb Blood Flow Metab, 2018. **38**(9): p. 1500-1516.

8.   Hu, H.J. and M. Song, *Disrupted Ionic Homeostasis in Ischemic Stroke and New Therapeutic Targets.* J Stroke Cerebrovasc Dis, 2017. **26**(12): p. 2706-2719.

9.   Mayor, D. and M. Tymianski, *Neurotransmitters in the mediation of cerebral ischemic injury.* Neuropharmacology, 2018. **134**(Pt B): p. 178-188.

10.   Mracskó, É., et al., *Oxidatív hatások és hatékony antioxidáns terápiás beavatkozások kísérletes agyi ischaemiában* in *Vasculáris neurológia.* 2011. p. 9.

11.   Thomas, R.C., *The plasma membrane calcium ATPase (PMCA) of neurones is electroneutral and exchanges 2 H+ for each Ca2+ or Ba2+ ion extruded.* J Physiol, 2009. **587**(2): p. 315-27.

12.   Brini, M., et al., *Neuronal calcium signaling: function and dysfunction.* Cell Mol Life Sci, 2014. **71**(15): p. 2787-814.

13.   Hossmann, K.A., *Viability thresholds and the penumbra of focal ischemia.* Ann Neurol, 1994. **36**(4): p. 557-65.

14.   Leao, A., *Spreading depression of activity in the cerebral cortex.* 1944: J Neurophys. p. 359-90.

15.   LEAO, A.A., *Further observations on the spreading depression of activity in the cerebral cortex.* J Neurophysiol, 1947. **10**(6): p. 409-14.

16.   Hossmann, K.A., *Periinfarct depolarizations.* Cerebrovasc Brain Metab Rev, 1996. **8**(3): p. 195-208.

17.   Nedergaard, M., *Spreading depression as a contributor to ischemic brain damage.* Adv Neurol, 1996. **71**: p. 75-83; discussion 83-4.

18.   Woitzik, J., et al., *Propagation of cortical spreading depolarization in the human cortex after malignant stroke.* Neurology, 2013. **80**(12): p. 1095-102.

19.   Pinczolits, A., et al., *Standard-sampling microdialysis and spreading depolarizations in patients with malignant hemispheric stroke.* J Cereb Blood Flow Metab, 2017. **37**(5): p. 1896-1905.

20.   Dreier, J.P., *The role of spreading depression, spreading depolarization and spreading ischemia in neurological disease.* Nat Med, 2011. **17**(4): p. 439-47.

21.   Hartings, J.A., et al., *The continuum of spreading depolarizations in acute cortical lesion development: Examining Leão's legacy.* J Cereb Blood Flow Metab, 2017. **37**(5): p. 1571-1594.

22.   Van Harreveld, A. and E. Fifková, *Glutamate release from the retina during spreading depression.* J Neurobiol, 1970. **2**(1): p. 13-29.

23.   Hansen, A.J., *Extracellular potassium concentration in juvenile and adult rat brain cortex during anoxia.* Acta Physiol Scand, 1977. **99**(4): p. 412-20.

24.   Somjen, G.G., *Mechanisms of spreading depression and hypoxic spreading depression-like depolarization.* Physiol Rev, 2001. **81**(3): p. 1065-96.

25.   von Bornstädt, D., et al., *Supply-demand mismatch transients in susceptible peri-infarct hot zones explain the origins of spreading injury depolarizations.* Neuron, 2015. **85**(5): p. 1117-31.

26.   Pietrobon, D. and M.A. Moskowitz, *Chaos and commotion in the wake of cortical spreading depression and spreading depolarizations.* Nat Rev Neurosci, 2014. **15**(6): p. 379-93.

27.   Ayata, C. and M. Lauritzen, *Spreading Depression, Spreading Depolarizations, and the Cerebral Vasculature.* Physiol Rev, 2015. **95**(3): p. 953-93.

28.   Ayata, C., *Spreading depression and neurovascular coupling.* Stroke, 2013. **44**(6 Suppl 1): p. S87-9.

29.   Dreier, J.P., et al., *Recording, analysis, and interpretation of spreading depolarizations in neurointensive care: Review and recommendations of the COSBID research group.* J Cereb Blood Flow Metab, 2017. **37**(5): p. 1595-1625.

30.   Klass, A., R. Sánchez-Porras, and E. Santos, *Systematic review of the pharmacological agents that have been tested against spreading depolarizations.* J Cereb Blood Flow Metab, 2018. **38**(7): p. 1149-1179.

31.   Hoffmann, U. and C. Ayata, *Neurovascular coupling during spreading depolarizations.* Acta Neurochir Suppl, 2013. **115**: p. 161-5.

32.   Siesjö, B.K., *Pathophysiology and treatment of focal cerebral ischemia. Part I: Pathophysiology.* J Neurosurg, 1992. **77**(2): p. 169-84.

33.   Rehncrona, S., *Brain acidosis.* Ann Emerg Med, 1985. **14**(8): p. 770-6.

34.   Paschen, W., et al., *Lactate and pH in the brain: association and dissociation in different pathophysiological states.* J Neurochem, 1987. **48**(1): p. 154-9.

35.   Katsura, K., et al., *Extracellular pH in the brain during ischemia: relationship to the severity of lactic acidosis.* J Cereb Blood Flow Metab, 1991. **11**(4): p. 597-9.

36.   von Hanwehr, R., M.L. Smith, and B.K. Siesjö, *Extra- and intracellular pH during near-complete forebrain ischemia in the rat.* J Neurochem, 1986. **46**(2): p. 331-9.

37.   Kraig, R.P., W.A. Pulsinelli, and F. Plum, *Carbonic acid buffer changes during complete brain ischemia.* Am J Physiol, 1986. **250**(3 Pt 2): p. R348-57.

38.   Plum, F., R.P. Kraig, and W.A. Pulsinelli, *Compartmentation of acid-base balance in brain during complete ischemia.* Neurochem Pathol, 1988. **9**: p. 139-44.

39.   Boris-Möller, F., et al., *Evidence against major compartmentalization of H+ in ischemic rat brain tissue.* Neurosci Lett, 1988. **85**(1): p. 113-8.

40.   Menyhárt, Á., et al., *Spreading depolarization remarkably exacerbates ischemia-induced tissue acidosis in the young and aged rat brain.* Sci Rep, 2017. **7**(1): p. 1154.

41.   Walz, W. and S. Mukerji, *Lactate release from cultured astrocytes and neurons: a comparison.* Glia, 1988. **1**(6): p. 366-70.

42.   Behar, K.L., D.L. Rothman, and K.A. Hossmann, *NMR spectroscopic investigation of the recovery of energy and acid-base homeostasis in the cat brain after prolonged ischemia.* J Cereb Blood Flow Metab, 1989. **9**(5): p. 655-65.

43.   Kobatake, K., et al., *Autoradiographic determination of brain pH following middle cerebral artery occlusion in the rat.* Stroke, 1984. **15**(3): p. 540-7.

44.   Back, T., et al., *Penumbral tissue alkalosis in focal cerebral ischemia: relationship to energy metabolism, blood flow, and steady potential.* Ann Neurol, 2000. **47**(4): p. 485-92.

45.   Mutch, W.A. and A.J. Hansen, *Extracellular pH changes during spreading depression and cerebral ischemia: mechanisms of brain pH regulation.* J Cereb Blood Flow Metab, 1984. **4**(1): p. 17-27.

46.   Scheller, D., J. Kolb, and F. Tegtmeier, *Lactate and pH change in close correlation in the extracellular space of the rat brain during cortical spreading depression.* Neurosci Lett, 1992. **135**(1): p. 83-6.

47.   Selman, W.R., et al., *Compromised metabolic recovery following spontaneous spreading depression in the penumbra.* Brain Res, 2004. **999**(2): p. 167-74.

48.   Menyhárt, Á., et al., *Age or ischemia uncouples the blood flow response, tissue acidosis, and direct current potential signature of spreading depolarization in the rat brain.* Am J Physiol Heart Circ Physiol, 2017. **313**(2): p. H328-H337.

49.   Dreier, J.P. and C. Reiffurth, *The stroke-migraine depolarization continuum.* Neuron, 2015. **86**(4): p. 902-922.

50.   Ay, H., et al., *Conversion of ischemic brain tissue into infarction increases with age.* Stroke, 2005. **36**(12): p. 2632-6.

51.   Magistretti, P.J. and I. Allaman, *Lactate in the brain: from metabolic end-product to signalling molecule.* Nat Rev Neurosci, 2018. **19**(4): p. 235-249.

52.   Feuerstein, D., et al., *Dynamic metabolic response to multiple spreading depolarizations in patients with acute brain injury: an online microdialysis study.* J Cereb Blood Flow Metab, 2010. **30**(7): p. 1343-55.

53.   Feuerstein, D., et al., *Regulation of cerebral metabolism during cortical spreading depression.* J Cereb Blood Flow Metab, 2016. **36**(11): p. 1965-1977.

54.   Nedergaard, M., et al., *Acid-induced death in neurons and glia.* J Neurosci, 1991. **11**(8): p. 2489-97.

55.   Gleichmann, M. and M.P. Mattson, *Neuronal calcium homeostasis and dysregulation.* Antioxid Redox Signal, 2011. **14**(7): p. 1261-73.

56.   Simms, B.A. and G.W. Zamponi, *Neuronal voltage-gated calcium channels: structure, function, and dysfunction.* Neuron, 2014. **82**(1): p. 24-45.

57.   Jackson, W.F., *Potassium Channels in Regulation of Vascular Smooth Muscle Contraction and Growth.* Adv Pharmacol, 2017. **78**: p. 89-144.

58.   Tomassoni, D., et al., *Nimodipine and its use in cerebrovascular disease: evidence from recent preclinical and controlled clinical studies.* Clin Exp Hypertens, 2008. **30**(8): p. 744-66.

59.   Steen, P.A., et al., *Nimodipine improves cerebral blood flow and neurologic recovery after complete cerebral ischemia in the dog.* J Cereb Blood Flow Metab, 1983. **3**(1): p. 38-43.

60.   Germano, I.M., et al., *The therapeutic value of nimodipine in experimental focal cerebral ischemia. Neurological outcome and histopathological findings.* J Neurosurg, 1987. **67**(1): p. 81-7.

61.   Pisani, A., et al., *L-type Ca2+ channel blockers attenuate electrical changes and Ca2+ rise induced by oxygen/glucose deprivation in cortical neurons.* Stroke, 1998. **29**(1): p. 196-201; discussion 202.

62.   Richter, F., A. Ebersberger, and H.G. Schaible, *Blockade of voltage-gated calcium channels in rat inhibits repetitive cortical spreading depression.* Neurosci Lett, 2002. **334**(2): p. 123-6.

63.   Menyhárt, Á., et al., *Large-conductance Ca.* Neurobiol Dis, 2018. **119**: p. 41-52.

64.   Szabó, Í., et al., *The impact of dihydropyridine derivatives on the cerebral blood flow response to somatosensory stimulation and spreading depolarization.* Br J Pharmacol, 2019. **176**(9): p. 1222-1234.

65. Dreier, J.P., et al., *Nitric oxide scavenging by hemoglobin or nitric oxide synthase inhibition by N-nitro-L-arginine induces cortical spreading ischemia when K+ is increased in the subarachnoid space.* J Cereb Blood Flow Metab, 1998. **18**(9): p. 978-90.

66. Windmüller, O., et al., *Ion changes in spreading ischaemia induce rat middle cerebral artery constriction in the absence of NO.* Brain, 2005. **128**(Pt 9): p. 2042-51.

67. Allen, G.S., et al., *Cerebral arterial spasm--a controlled trial of nimodipine in patients with subarachnoid hemorrhage.* N Engl J Med, 1983. **308**(11): p. 619-24.

68. *Clinical trial of nimodipine in acute ischemic stroke. The American Nimodipine Study Group.* Stroke, 1992. **23**(1): p. 3-8.

69. Fagan, S.C., et al., *Effect of nimodipine on blood pressure in acute ischemic stroke in humans.* Stroke, 1988. **19**(3): p. 401-2.

70. Thirugnanachandran, T., et al., *Refining the ischemic penumbra with topography.* Int J Stroke, 2018. **13**(3): p. 277-284.

71. Carradori, D., et al., *Application of Nanomedicine to the CNS Diseases.* Int Rev Neurobiol, 2016. **130**: p. 73-113.

72. Oishi, M. and Y. Nagasaki, *Stimuli-responsive smart nanogels for cancer diagnostics and therapy.* Nanomedicine (Lond), 2010. **5**(3): p. 451-68.

73. Liu, J., et al., *pH-sensitive nano-systems for drug delivery in cancer therapy.* Biotechnol Adv, 2014. **32**(4): p. 693-710.

74. Janovák, L., et al., *Preparation of novel tissue acidosis-responsive chitosan drug nanoparticles: Characterization and in vitro release properties of Ca.* Eur J Pharm Sci, 2018. **123**: p. 79-88.

75. Tóth, O.M., et al., *Chitosan nanoparticles release nimodipine in response to tissue acidosis to attenuate spreading depolarization evoked during forebrain ischemia.* Neuropharmacology, 2020. **162**: p. 107850.

76. Voipio, J. and K. Kaila, *Interstitial PCO2 and pH in rat hippocampal slices measured by means of a novel fast CO2/H(+)-sensitive microelectrode based on a PVC-gelled membrane.* Pflugers Arch, 1993. **423**(3-4): p. 193-201.

77. Faulkner, S., et al., *Xenon augmented hypothermia reduces early lactate/N-acetylaspartate and cell death in perinatal asphyxia.* Ann Neurol, 2011. **70**(1): p. 133-50.

78. Varga, V., et al., *Molecular hydrogen alleviates asphyxia-induced neuronal cyclooxygenase-2 expression in newborn pigs.* Acta Pharmacol Sin, 2018. **39**(8): p. 1273-1283.

79. Farkas, E., et al., *Direct, live imaging of cortical spreading depression and anoxic depolarisation using a fluorescent, voltage-sensitive dye.* J Cereb Blood Flow Metab, 2008. **28**(2): p. 251-62.

80. Dreier, J.P., et al., *Ischemia triggered by red blood cell products in the subarachnoid space is inhibited by nimodipine administration or moderate volume expansion/hemodilution in rats.* Neurosurgery, 2002. **51**(6): p. 1457-65; discussion 1465-7.

81. Freedman, D.D. and D.D. Waters, *'Second generation' dihydropyridine calcium antagonists. Greater vascular selectivity and some unique applications.* Drugs, 1987. **34**(5): p. 578-98.

82. Scriabine, A., T. Schuurman, and J. Traber, *Pharmacological basis for the use of nimodipine in central nervous system disorders.* FASEB J, 1989. **3**(7): p. 1799-806.

83. Martínez-Vila, E., et al., *Placebo-controlled trial of nimodipine in the treatment of acute ischemic cerebral infarction.* Stroke, 1990. **21**(7): p. 1023-8.

84.   Harper, A.M., L. Craigen, and S. Kazda, *Effect of the calcium antagonist, nimodipine, on cerebral blood flow and metabolism in the primate.* J Cereb Blood Flow Metab, 1981. **1**(3): p. 349-56.

85.   Wong, H.L., X.Y. Wu, and R. Bendayan, *Nanotechnological advances for the delivery of CNS therapeutics.* Adv Drug Deliv Rev, 2012. **64**(7): p. 686-700.

86.   Bonnard, T., et al., *Recent Advances in Nanomedicine for Ischemic and Hemorrhagic Stroke.* Stroke, 2019. **50**(5): p. 1318-1324.

87.   Gilmore, J.L., et al., *Novel nanomaterials for clinical neuroscience.* J Neuroimmune Pharmacol, 2008. **3**(2): p. 83-94.

88.   Kyle, S. and S. Saha, *Nanotechnology for the detection and therapy of stroke.* Adv Healthc Mater, 2014. **3**(11): p. 1703-20.

89.   Amani, H., et al., *Antioxidant nanomaterials in advanced diagnoses and treatments of ischemia reperfusion injuries.* J Mater Chem B, 2017. **5**(48): p. 9452-9476.

90.   Chen, L. and X. Gao, *The application of nanoparticles for neuroprotection in acute ischemic stroke.* Ther Deliv, 2017. **8**(10): p. 915-928.

91.   Kaviarasi, S., et al., *Emerging paradigms in nanotechnology for imaging and treatment of cerebral ischemia.* J Control Release, 2019. **300**: p. 22-45.

92.   Luo, Z., et al., *Mesoporous silica nanoparticles end-capped with collagen: redox-responsive nanoreservoirs for targeted drug delivery.* Angew Chem Int Ed Engl, 2011. **50**(3): p. 640-3.

93.   Felber, A.E., M.H. Dufresne, and J.C. Leroux, *pH-sensitive vesicles, polymeric micelles, and nanospheres prepared with polycarboxylates.* Adv Drug Deliv Rev, 2012. **64**(11): p. 979-92.

94.   Zhai, J., et al., *Metal-Ion-Responsive Bionanocomposite for Selective and Reversible Enzyme Inhibition.* J Am Chem Soc, 2018. **140**(49): p. 16925-16928.

95.   Kwon, E.J., J.H. Lo, and S.N. Bhatia, *Smart nanosystems: Bio-inspired technologies that interact with the host environment.* Proc Natl Acad Sci U S A, 2015. **112**(47): p. 14460-6.

96.   Thistlethwaite, A.J., et al., *pH distribution in human tumors.* Int J Radiat Oncol Biol Phys, 1985. **11**(9): p. 1647-52.

97.   Martin, G.R. and R.K. Jain, *Noninvasive measurement of interstitial pH profiles in normal and neoplastic tissue using fluorescence ratio imaging microscopy.* Cancer Res, 1994. **54**(21): p. 5670-4.

98.   Engin, K., et al., *Extracellular pH distribution in human tumours.* Int J Hyperthermia, 1995. **11**(2): p. 211-6.

99.   Shenoy, D., et al., *Poly(ethylene oxide)-modified poly(beta-amino ester) nanoparticles as a pH-sensitive system for tumor-targeted delivery of hydrophobic drugs: part 2. In vivo distribution and tumor localization studies.* Pharm Res, 2005. **22**(12): p. 2107-14.

100.   Poon, Z., et al., *Layer-by-layer nanoparticles with a pH-sheddable layer for in vivo targeting of tumor hypoxia.* ACS Nano, 2011. **5**(6): p. 4284-92.

101.   Kandell, R.M., L.E. Waggoner, and E.J. Kwon, *Nanomedicine for Acute Brain Injuries: Insight from Decades of Cancer Nanomedicine.* Mol Pharm, 2021. **18**(2): p. 522-538.

102.   Li, X., et al., *Chitin, chitosan, and glycated chitosan regulate immune responses: the novel adjuvants for cancer vaccine.* Clin Dev Immunol, 2013. **2013**: p. 387023.

103.   Carroll, E.C., et al., *The Vaccine Adjuvant Chitosan Promotes Cellular Immunity via DNA Sensor cGAS-STING-Dependent Induction of Type I Interferons.* Immunity, 2016. **44**(3): p. 597-608.

104.   Liu, Y., et al., *Effects of engineered nanoparticles on the innate immune system.* Semin Immunol, 2017. **34**: p. 25-32.

105. Shen, Y., et al., *pH-responsive nanoparticles for cancer drug delivery.* Methods Mol Biol, 2008. **437**: p. 183-216.
106. Varga, D.P., et al., *Contribution of prostanoid signaling to the evolution of spreading depolarization and the associated cerebral blood flow response.* Sci Rep, 2016. **6**: p. 31402.
107. Menyhárt, Á., et al., *High incidence of adverse cerebral blood flow responses to spreading depolarization in the aged ischemic rat brain.* Neurobiol Aging, 2015. **36**(12): p. 3269-3277.
108. Cox, S.B., T.A. Woolsey, and C.M. Rovainen, *Localized dynamic changes in cortical blood flow with whisker stimulation corresponds to matched vascular and neuronal architecture of rat barrels.* J Cereb Blood Flow Metab, 1993. **13**(6): p. 899-913.
109. Iadecola, C., *The Neurovascular Unit Coming of Age: A Journey through Neurovascular Coupling in Health and Disease.* Neuron, 2017. **96**(1): p. 17-42.
110. Attwell, D., et al., *Glial and neuronal control of brain blood flow.* Nature, 2010. **468**(7321): p. 232-43.
111. Cheli, V.T., et al., *L-type voltage-operated calcium channels contribute to astrocyte activation In vitro.* Glia, 2016. **64**(8): p. 1396-415.
112. Richter, F., et al., *Tumor necrosis factor reduces the amplitude of rat cortical spreading depression in vivo.* Ann Neurol, 2014. **76**(1): p. 43-53.
113. Reinhart, K.M. and C.W. Shuttleworth, *Ketamine reduces deleterious consequences of spreading depolarizations.* Exp Neurol, 2018. **305**: p. 121-128.
114. Bielenberg, G.W., et al., *Effects of nimodipine on infarct size and cerebral acidosis after middle cerebral artery occlusion in the rat.* Stroke, 1990. **21**(12 Suppl): p. IV90-2.
115. Berger, L. and A.M. Hakim, *Calcium channel blockers correct acidosis in ischemic rat brain without altering cerebral blood flow.* Stroke, 1988. **19**(10): p. 1257-61.
116. Bielenberg, G.W., H. Haubruck, and J. Krieglstein, *Effects of calcium entry blocker emopamil on postischemic energy metabolism of the isolated perfused rat brain.* J Cereb Blood Flow Metab, 1987. **7**(4): p. 489-96.
117. Furtado, D., et al., *Overcoming the Blood-Brain Barrier: The Role of Nanomaterials in Treating Neurological Diseases.* Adv Mater, 2018. **30**(46): p. e1801362.
118. Sarvaiya, J. and Y.K. Agrawal, *Chitosan as a suitable nanocarrier material for anti-Alzheimer drug delivery.* Int J Biol Macromol, 2015. **72**: p. 454-65.
119. Wilson, B., et al., *Chitosan nanoparticles as a new delivery system for the anti-Alzheimer drug tacrine.* Nanomedicine, 2010. **6**(1): p. 144-52.
120. Aktaş, Y., et al., *Development and brain delivery of chitosan-PEG nanoparticles functionalized with the monoclonal antibody OX26.* Bioconjug Chem, 2005. **16**(6): p. 1503-11.
121. Yemişci, M., et al., *Transport of a caspase inhibitor across the blood-brain barrier by chitosan nanoparticles.* Methods Enzymol, 2012. **508**: p. 253-69.
122. Jiang, X., et al., *Blood-brain barrier dysfunction and recovery after ischemic stroke.* Prog Neurobiol, 2018. **163-164**: p. 144-171.
123. Cottier, K.E., et al., *Loss of Blood-Brain Barrier Integrity in a KCl-Induced Model of Episodic Headache Enhances CNS Drug Delivery.* eNeuro, 2018. **5**(4).
124. Sadeghian, H., et al., *Spreading depolarizations trigger caveolin-1-dependent endothelial transcytosis.* Ann Neurol, 2018. **84**(3): p. 409-423.
125. Joshi, S., P.M. Meyers, and E. Ornstein, *Intracarotid delivery of drugs: the potential and the pitfalls.* Anesthesiology, 2008. **109**(3): p. 543-64.
126. Yu, S., et al., *Chitosan and chitosan coating nanoparticles for the treatment of brain disease.* Int J Pharm, 2019. **560**: p. 282-293.

127. Dodane, V., M. Amin Khan, and J.R. Merwin, *Effect of chitosan on epithelial permeability and structure.* Int J Pharm, 1999. **182**(1): p. 21-32.
128. Smith, J., E. Wood, and M. Dornish, *Effect of chitosan on epithelial cell tight junctions.* Pharm Res, 2004. **21**(1): p. 43-9.